

The gas hydrate system of the western Black Sea Basin

Ewa Burwicz-Galerne^{a,*}, Matthias Haeckel^b, Christian Hensen^b, Rohit Samant^c, Klaus Wallmann^b

^a MARUM – Center for Marine Environmental Sciences, University of Bremen, Leobener Str. 8, 28359, Bremen, Germany

^b GEOMAR Helmholtz Centre for Ocean Research Kiel, Wischhofstr. 1-3, 24148, Kiel, Germany

^c University of Münster, Münster, Germany

ARTICLE INFO

Keywords:

Black Sea
Gas hydrate
Methane
3D basin model
High sedimentation
Danube fan
Dniepr fan
Offshore Turkey

ABSTRACT

The basin-scale distribution of gas hydrates and methane migration pathways in the western Black Sea remains enigmatic, owing to the region's complex geological history. Characterizing the abundant gas hydrate accumulations across temporal scales poses significant challenges. In this study, we developed and applied a 3D large-scale numerical model to study the formation, development, and fate of natural gas hydrate systems in the western Black Sea sub-basin. Our model enables us to simulate the dynamic evolution of basin geometry and facies distribution over the last 98 million years and under dynamically changing boundary conditions, e.g. due to sea-level changes. Our study estimates the total volume of gas hydrates stored within western Black Sea sediments at $\sim 14,607$ MtC, equivalent to $\sim 30,073 \times 10^{11} \text{ m}^3$ of CH_4 (at STP conditions) which is about 5 times higher than average gas hydrate density at continental margins. Our findings reveal three distinct mechanisms driving gas hydrate reservoir formation within the reconstructed sub-basin: gas hydrate recycling zones, chimney-like structure formation, and gas hydrate deposits associated with paleo-deep sea fans. We identified and simulated key controlling parameters, related to methane migration pathways and regional geomorphology, governing each type of hydrate formation. Subsequently, we conduct a detailed analysis of regional gas hydrate systems, focusing on the Dniepr paleo-fan system, the Danube paleo-fan region, multiple offshore locations near Turkey, and the central Black Sea area. Furthermore, we investigate various biogenic methane formation kinetics and their impact on basin-scale methane generation. Our sensitivity studies enable us to predict the optimal temperature range for microbial activity driving methanogenesis in the Black Sea sediments at 30°C – 40°C . Overall, our study provides a novel understanding and quantitative correlation between methane generation, migration, and storage in the form of gas hydrates on a basin-scale in the western Black Sea.

1. Introduction

Natural gas hydrate systems serve as both, sources and sinks of light hydrocarbon gases, predominantly methane, which are locked within crystalline lattice structures formed by water molecules. Submarine gas hydrates are commonly found in low-temperature, high-pressure environments with substantial methane generation, such as the continental shelf (in water depths exceeding 300 m) and continental slope. The gas hydrate formation mechanism requires the presence of sufficient amounts of gas that can be trapped within the cage structure. While natural gas hydrate deposits are abundant (Burwicz et al., 2011; Milkov, 2004; Wallmann et al., 2012), they remain susceptible to external factors controlling the spatial extent of the gas hydrate stability zone (GHSZ) in marine sediments, such as changes in water depth, bottom-water

temperature (Biaśtoch et al., 2011; Kretschmer et al., 2015), sedimentation rates (Gupta et al., 2023, 2024; Schmidt et al., 2022; Zander et al., 2017) and erosion (Wallmann et al., 2018).

The current assessment of gas hydrate deposits in the Black Sea relies on relatively sparse regional data. This geological setting is characterized by extremely high sedimentation rates and a complex thermal and sedimentological history, making basin-scale estimates on gas hydrate accumulations challenging. Given the significant spatial heterogeneity of the natural gas hydrate system in the Black Sea, our understanding of dominant gas hydrate formation mechanisms and methane migration pathways in the past and present remains limited.

The results of our study suggest that the western Black Sea sub-basin has undergone multiple phases of gas hydrate formation and dissociation due to fluctuations in sea-level, bottom-water temperature and

* Corresponding author.

E-mail address: eburwicz-galerne@marum.de (E. Burwicz-Galerne).

<https://doi.org/10.1016/j.marpetgeo.2024.107026>

Received 30 April 2024; Received in revised form 16 July 2024; Accepted 22 July 2024

Available online 31 July 2024

0264-8172/© 2024 The Author(s). Published by Elsevier Ltd. This is an open access article under the CC BY-NC license (<http://creativecommons.org/licenses/by-nc/4.0/>).

sedimentation rates. With a sediment cover thickness of up to 19 km, the Black Sea remains one of the deepest sedimentary basins in the world. These extremely high rates of sediment deposition have led to the entrapment of substantial organic matter, resulting in significant biogenic methane production, the primary methane source in the region. Our simulations demonstrate that gas hydrate deposit distribution in the western Black Sea sub-basin is highly heterogeneous and controlled by the complex interplay between external environmental factors like bottom-water temperature and sedimentation rates, and internal factors such as organic matter distribution and degradation rates.

In conclusion, our study provides new insights into the formation mechanisms and controlling factors of gas hydrate deposits in the western Black Sea sub-basin. Our results have important implications for estimating gas hydrate reserves in the region and assessing the global gas hydrate budget and carbon cycle.

2. The study area

The western part of the Black Sea basin (see Fig. 1) is an example of a back-arc basin with exceptionally high sedimentation rates and complex geometry. Its formation started in the late Cretaceous approximately 98 Ma ago, situated between the subducting Tethys Ocean and the Eurasian tectonic plate (Robinson et al., 1996). Presently, the deepest central parts of the basin reach water depths of ~2,200 m, with a sediment cover of up to 18.5 km. The southern and eastern rims of the western

Black Sea are characterized by relatively narrow continental shelves and abrupt shelf breaks. In contrast, the northern and northwestern Black Sea shelves are wider and renowned for hosting a large variety of geological features, including abundant methane seepage sites, gas hydrates, and mud volcanoes, particularly towards the central and eastern side of the Crimean Peninsula. Anoxic sediments in the Black Sea facilitate organic matter preservation in deeper sediment layers, creating significantly higher burial efficiency conditions (Li et al., 2023). In these favorable settings, the majority of methane in the Black Sea is of biogenic origin and is produced in-situ through organic matter degradation processes (Bialas and Haeckel, 2022; Minshull et al., 2020; Pape et al., 2008, 2020). The possibility of thermogenic methane as a source for the Black Sea gas hydrates was debated due to the presence of the organic-rich Oligocinian Maykop facies spread across the entire basin at depths ranging from 1,000 m in the shelf region up to 2,000 m in the basin center. However, as demonstrated in previous studies (Burwicz and Haeckel, 2020; Olaru et al., 2018), due to the thermally immature state of the Maykop series, no significant portion of thermogenic methane is produced in the deeper basin strata. Large amounts of in-situ produced microbial methane seep out from the seafloor alongside the Black Sea shelves where gas hydrates are thermodynamically unstable. The remaining methane generated on a basin-scale saturates the pore fluids and migrates towards the upper hundreds of meters, accumulating in the form of gas hydrates.

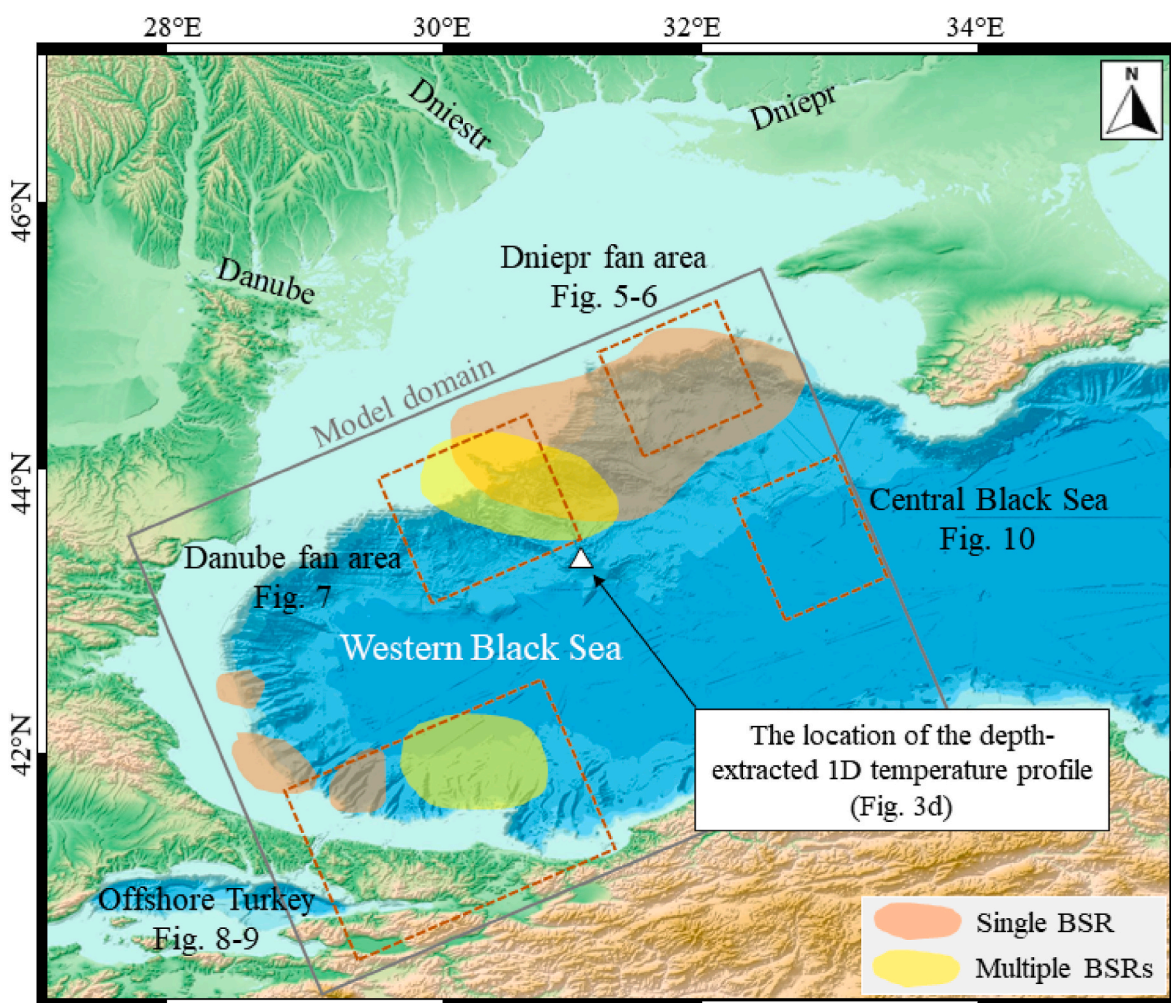


Fig. 1. Bathymetry map of the western Black Sea basin showing the 3D model domain and four regions of interest discussed in this study. Gridded bathymetry data are provided by the GEBCO (GEBCO, Compilation, Group, 2023) with a resolution of 15 arc-seconds. The areas with evidence of the presence of single or multiple bottom simulating reflectors (BSRs) are compiled after Bialas and Haeckel (2022).

Throughout the history of the Black Sea, multiple events of low and high sea-level stands, known as limnic and marine stages related to the opening and closing of the Bosphorus strait, have occurred. Today dense saline waters remain in the lower part of the water column, while fresher waters dominate towards the sea surface, creating a steep halocline at approximately 90 m water depth. The northern part of the basin is renowned for its abundant river delta and paleo-delta systems associated with multiple major rivers, including the Danube, Dniepr, and Dniestr, which deliver significant amounts of organic-rich clastic material towards the deeper basin parts, primarily during sea-level lowstands. The extent of these major rivers' paleo-delta systems reaches hundreds of kilometers in length and significantly shapes the regional basin geometry, providing important structural components of the subseafloor, such as canyons with overbanks, ridges, terraces, channel floors, and flanks.

Previous estimates based on gas hydrate stability zone thickness, steady-state conditions, and biogenic methane sources (Vassilev and Dimitrov, 2002) suggest a gas hydrate inventory for the entire Black Sea region ranging from 77 to $350 \times 10^9 \text{ m}^3$ of hydrate, equivalent to $10\text{--}50 \times 10^{12} \text{ m}^3$ of methane gas at standard temperature-pressure conditions (STP), indicating potentially high local economic significance of the region (Minshull et al., 2020). The western part of the Black Sea basin is also characterized by abundant gas seepage sites and associated mud volcanos (Starostenko et al., 2010). Basin-scale estimates on the methane mission rates from the seafloor to the water column suggest that approximately $3.60\text{--}5.65 \text{ Tg yr}^{-1}$ of CH_4 is emitted from the seeps and decomposing gas hydrates (Kessler et al., 2006). However, the majority of the released methane is most likely buffered by microbial methane consumption and hydrographic stratification in the water column (Schmale et al., 2011).

3. Materials and methods

3.1. Basin-scale numerical model

We used the commercial petroleum system modelling software PetroMod v.2023.1 by Schlumberger (Hantschel and Kauerauf, 2009) for this study. Here, we provide detailed explanations of the modelling assumptions related to both microbial and thermogenic gas formation, facies distribution, and gas hydrate formation in the model. The 3D back-stripping basin restoration technique was previously used as a generic model framework in the study by Burwicz and Haeckel (2020) and Burwicz et al. (2017). The lateral dimensions of the model are approximately 500 by 500 km^2 , with a grid resolution of 280 by 260 nodes, resulting in an XY resolution of about 1.8 by 1.9 km^2 (see Fig. 2). The choice made on the lateral grid resolution does not affect the results of the simulation; however, it affects the amount of computational time required to perform each simulation run. The chosen grid allows us to resolve the majority of geometrical features identified on interpreted seismic without expanding the computational time. In case of the upper most layers, bathymetric features of the seafloor have been initially resolved using the extracted 2D topography map from the global GEBCO dataset with a 15 arc-second resolution (GEBCO, Compilation, Group, 2023) and subsequently re-gridded to match the final XY model resolution.

The vertical dimension varies depending on the basin geometry, reaching about 18 km at the deepest basin center. Therefore, vertical model resolution changes in space and time, typically ranging from 100 to 400 m for the deeper part of the sedimentary column, up to 2 m resolution in the uppermost sediment section inside and hundred meters

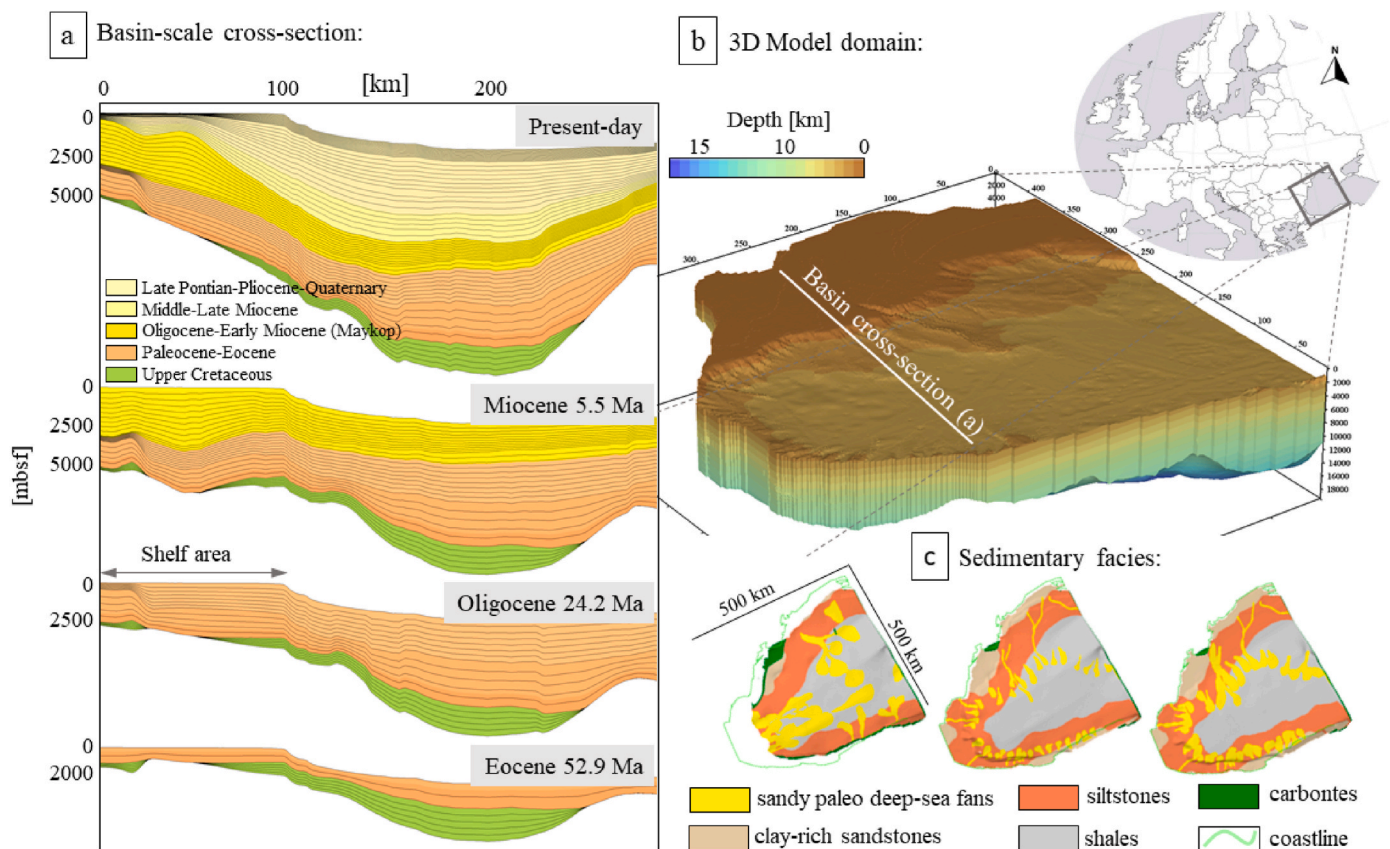


Fig. 2. A) Basin-scale cross-section presenting the western Black Sea basin evolution simulated in our model with a back-stripping method as four snapshots from Eocene to the present-day, b) Location and geometry of the model reconstructed from seismic interpretation of 103 horizons (Nikishin et al., 2015), c) spatial distribution of sedimentary facies defined in the model at three stratigraphic levels from Oligocene (left) to Quaternary (right) (figure inserts modified after Burwicz and Haeckel (2020)).

below the gas hydrate stability zone. The GHSZ in the software is calculated according to the deepest cell that lies entirely within GHSZ limits, therefore, having larger grid cells would lead to underestimating of the overall GHSZ thickness and, consequently, the gas hydrate inventory. Moreover, such high resolution in the upper section is required to match simulated results with the observed BSR depths and other hydrate and gas presence indicators.

The model consists of a total of 4.222 million cells populated with various facies and 58 sedimentary layers, the properties of which are summarized in Table 1. The time-step of the numerical simulation generally depends on the thickness of deposited sedimentary package and cannot exceed 10 Ma. It is also constrained by the temporal resolution of the paleo-water depth and paleo-bottom water temperature records. For the most recent geological history with multiple glacial and interglacial periods, the maximum time-step was limited to 1,000 a. Overall, each modeling scenario has been simulated on a local 8 cores/10 processors workstation with 32 GB of physical memory (RAM) for about 20 h in a full 3D migration mode, generating ~180 GB of output data.

3.2. Lithostratigraphy and facies description

The model contains 40 sedimentary layers stretched between the crystalline basement and the seafloor. The oldest sedimentary layers are Cretaceous in age deposited on top of post-rift basement (98 Ma). Lithostratigraphic properties of sedimentary layers (i.e. seafloor porosity, compaction length scale, thermal conductivity etc.) used in the model and summarized in Table 1 are based on the values compiled in the PetroMod software library (Hantschel and Kauerauf, 2009). Mixed lithologies (e.g. carbonates, marls etc.) in a single sedimentary package result in averaged mechanical and thermal properties of numerical layers. However, the initial content of total organic carbon (TOC) and hydrogen index (HI index; see Table 1) are defined separately (i.e. not averaged) for various facies included in one sedimentary package of a given age (e.g. Late Miocene) based on the results from Sachsenhofer et al. (2018), Mayer et al. (2018a), and Boote et al. (2018). The spatial distribution of facies is illustrated in Fig. 2 for three stratigraphic ages - Oligocene-Early Miocene, Middle Miocene, and Pliocene-Quaternary.

3.3. Methane sources in the model

Two sources of methane are considered in the model: in-situ biogenic POC degradation leading to biogenic methane formation, and source rock thermal maturation at great depths leading to thermogenic methane formation. The high-resolution 3D model relies on the input from the large basin-scale simulation presented by Burwicz and Haeckel (2020). To correctly estimate the volume and mobility of hydrocarbon components (including gas hydrate-forming methane), the large-scale model covers the entire western Black Sea sub-basin. Generated and expelled gas masses are free to migrate from the source rock towards the reservoir locations, which, in this particular case, are presented as sandy paleo-levee delta systems. Specifically, organic-rich Maykop facies in the central part of the western Black Sea basin were thought to generate large amounts of thermogenic methane gas that migrates along the carrier beds towards the slope and shelf region, where coarse sediments of the paleo-delta channels provide a potential gas hydrate reservoir (Mayer et al., 2018b). The results from Burwicz and Haeckel (2020) predicts that the majority of the Maykop facies remains pre-mature and therefore not yet productive, which is in agreement with observations of wide-spread biogenic methane accumulations in the western Black Sea region (Greinert et al., 2010; Haeckel et al., 2015; Pape et al., 2008; Popescu et al., 2007; Römer et al., 2020). In this study, we support the conclusions of Mayer et al. (2018b) and Burwicz and Haeckel (2020) that only a limited part of the Maykopian shale formation located in the central part of the Black Sea basin reached the maturity window to generate oil and thermogenic gas. We attribute thermogenic

components predicted at the present-day in the shallow-water areas to the efficient lateral migration process.

3.3.1. Biogenic methane generation kinetics

Depth-decreasing reactivity of metabolites leading to in-situ biogenic methane formation based on Middelburg organic carbon degradation kinetics (Middelburg, 1989) is commonly used in numerical transport-reactive models (Burwicz and Rupke, 2019; Burwicz et al., 2011; Gupta et al., 2023, 2024; Schmidt et al., 2022; Treude et al., 2020; Wallmann et al., 2012) and was implemented in the commercial petroleum system software PetroMod to allow for biogenic methane generation (Burwicz and Haeckel, 2020; Burwicz et al., 2017; Hantschel and Kauerauf, 2009). However, the alternative modeling scenarios available in the software allow for the arbitrary choice of the main microbial reactivity window (Table 2). In Appendix A, we provide a set of sensitivity scenarios exploring the alternative paths of biogenic methane formation via temperature-dependent kinetics that assume a Gaussian-type reactivity distribution with the main activity peaks at 30 °C, 40 °C, 50 °C, 60 °C, and 70 °C to provide a comprehensive comparison between both modeling approaches.

3.4. Gas hydrate formation modeling

Gas hydrate crystallization occurs whenever local P-T conditions fall within the GHSZ and methane saturations exceed P-T-S-dependent solubility level. Pressure and temperature conditions which define the spatial extension of the GHSZ are calculated at each time-step and account for the changes in sedimentation, fluid and gas flow, sea-level fluctuations etc. The model allows the sediment pore space to be occupied by multiple methane-containing phases at the same moment, i.e. gas hydrate or free gas. Gas hydrate and free gas saturations predicted in the model are presented in vol % which indicates the portion of the pore space occupied by the specific component. The phase boundary zone between gas hydrate and free methane gas coincides with the lower GHSZ boundary. At this depth, a gas hydrate-free gas recycling process might occur in case of high burial rates pushing already formed hydrate deeper and outside the GHSZ. Instantaneous dissociation of hydrates releases methane gas which becomes mobile and migrates towards the seafloor, eventually re-entering the GHSZ and forming gas hydrate. The importance of these mechanisms, especially in high sedimentation regimes, was discussed in detail by Burwicz et al. (2017) on the Gulf of Mexico 3D modeling example. The only gas hydrate forming gas is methane, however, two fully miscible sources of CH₄ are accounted for in the model. Both biogenic and thermogenic methane are allowed to dissolve in pore fluids or form free methane gas and being transported towards the GHSZ where gas hydrates can be formed. However, it is only possible to track both components separately and distinguish between gas hydrate deposits of different gas origin at the initial stage of gas hydrate formation. Therefore, multiple events of gas hydrate dissolution and re-formation can only be investigated as a bulk gas hydrate volume of a mixed origin.

3.5. Model setup, boundary conditions, and calibration

Temperature calibration was performed against the compilation of the borehole data presented by Oлару et al. (2018) (green dots in Fig. 3d). The location of the 1D profile extraction point presented in Fig. 3d is marked in Fig. 1e. Collected borehole temperatures represent mostly shelf as well as the slope environments and therefore can be directly compared with our model predictions. Thermal conductivity measurements collected during the DSDP cruise Leg 42B from the Sites 380 and 381 (Erickson et al., 1978) were used to calibrate the model. Good correlation between the modeled curves and data points has been obtained for both parameters. Present-day as well as paleo-temperatures in the sediments are further constrained by mapped BSR depths. Interpreted to be the most recent (i.e. not necessarily thermally equilibrated)

Table 1
Lithostratigraphy and sediment properties used in the modeling study.

Era	Period	Epoch	Stage	Simulated regional sedimentary formations	Ages of simulated formations (Ma)	Lithology	Initial porosity (%)	Compaction length scale (1/km)	Thermal conductivity at 20 °C (W/mK)	Heat capacity at 20 °C (J/kgK)	Radioactive heat ($\mu\text{W}/\text{m}^3$)	TOC content (wt. %)	HI index (mgHC/gTOC)	
Cenozoic	Quaternary	Holocene	Lower/Middle/Upper											
			Upper											
		Pleistocene	Chibanian	Late Pontian-Pliocene-Quaternary	5.3–0	Mud-siltstone	70	0.83	1.64–2.05	860–910	2.03–0.96	0.5	123	
			Calabrian											
			Gelasian											
	Pliocene	Piacenzian												
		Zanclean												
	Neogene	Miocene	Messinian	Late Miocene: Meotian, Pontian, Dacian	11.60–5.3	Shales, marly shales, turbidite	67	0.83	1.77	860	1.78	0.5 (open-basin), 0 (shelf)	123 (open-basin), 0 (shelf)	
			Tortonian											
			Serravallian	Middle Miocene: Badenian, Sarmatian	20–11.6	Shales, marly shales, turbidite	67	0.83	1.77	860	1.78	0.5 (open-basin), 0 (shelf)	123 (open-basin), 0 (shelf)	
		Oligocene	Aquitanian	Oligocene-Early Miocene (Maykop)	33.9–20.0	Shales, turbidities	70	0.83	1.45	880	2.30	1.5	234	
			Chattian											
	Paleogene	Eocene	Rupelian											
			Priabonian											
			Bartonian	Eocene	55.8–33.9	Carbonates, marls, turbidite	48	0.5	2.30	850	0.89	0.5	123	
Lutetian														
Paleocene		Ypresian												
		Thanetian												
		Selandian	Paleocene	65.5–55.8	Carbonates, marls, turbidite	48	0.5	2.30	850	0.89	0.5	123		
Mesozoic	Cretaceous	Upper	Danian											
			Maastrichtian	Maastrichtian	70.6–65.5	Carbonates, marls, turbidite	48	0.5	2.30	850	0.89	0.3 (open-basin), 0 (shelf)	300 (open-basin), 0 (shelf)	
		Lower	Campanian	Campanian	83.5–70.6	Carbonates, marls, turbidite	48	0.5	2.30	850	0.89	0.3 (open-basin), 0 (shelf)	300 (open-basin), 0 (shelf)	
			Santonian	Late Santonian	85.8–83.5	Carbonates	48	0.5	2.30	850	0.89	0.3 (open-basin), 0 (shelf)	300 (open-basin), 0 (shelf)	
			Cenomanian-Early Santonian	98.0–85.8	Carbonates, marls, turbidite	48	0.5	2.30	850	0.89	0.3 (open-basin), 0 (shelf)	300 (open-basin), 0 (shelf)	Coniacian Turonian Cenomanian	

Table 2
Comparison of biogenic methane generation kinetics used in modelling studies.

Reference	Study Location	Model	Sediment Age	Kinetics/Mean Temperature	TOC (wt. %); HI (mgHC/gTOC)
This study	Western Black Sea basin	3D	Cretaceous to Recent	Middelburg kinetics/variable mean temperature	0.3–1.5; 123–300
Kroeger et al. (2015)	Pegasus Basin, New Zealand	2D	Miocene to Recent	37.5 °C	0.5 & 1.0; 100
Kroeger et al. (2019)	Hikurangi margin, New Zealand	3D	Neogene	37.5 °C	0.5 & 1.0; 100
Crutchley et al. (2017)	Hikurangi margin, New Zealand	2D	Miocene to Recent	37.5 °C	0.5; 100
Kroeger et al. (2017)	Taranaki Basin, New Zealand	2D	Miocene to Recent	37.5 °C	0.5; 100
Fujii et al. (2016)	Nankai Trough, Japan	2D 3D	1.5 to 0 Ma	12.5 °C	0.5; 60
Lyu et al. (2020)	Pearl River Mouth Basin, China	2D	Quaternary and older	55 °C	0.5 & 1.0; n/a
Pinero et al. (2016)	Theoretical layer-cake model	3D	2.5 to 0 Ma	Middelburg kinetics	2.5; 240
Burwicz et al. (2017)	Green Canyon, Gulf of Mexico	3D	Pliocene and Pleistocene	Middelburg kinetics	0.7 & 1.0; 100

BSR levels were used to cross-check predicted sediment temperatures (Gupta et al., 2024; Zander et al., 2017). In this study, we follow the interpretation of Tari et al. (2016), Krezsek et al. (2016), and Constantinescu et al. (2015) who argue for small to moderate (up to 600 m) sea-level drop related to the Messinian Salinity Crisis (MSC). Accordingly, no significant changes in the bottom water temperature as well as in the sea level conditions were imposed in the modeling periods before 20 ka BP and 28.5 ka BP, respectively.

4. Results and discussion

4.1. Gas hydrate inventory and formation mechanisms in the western Black Sea

Present-day and past gas hydrate inventories were predicted by the model. In this section, we analyze the results as a basin-scale inventory (part I) and with respect to the regional gas hydrate budgets (part II). In this study, we compare direct observations with our modeling results to establish the most probable scenario of a free gas migration within morphologically complex sediments of the Dniepr paleo delta system that led to gas hydrate formation and, furthermore, free gas migration and venting. In the section below, we discuss the following aspects of the gas hydrate system: spatial extent of the GHSZ, the location and origin of the gas seepage sites, potential free gas migration pathways, inferred locations and saturation of gas hydrate deposits, and the suggested presence of a free gas front.

4.1.1. Basin-scale inventory

Estimates by Vassilev and Dimitrov (2002) suggest that 91% of the deep Black Sea basin lies within the gas hydrate stability zone limits. However, these calculations were made under the assumption of equilibrated steady-state P-T-S conditions, i.e. excluding the potential effects of rapid sedimentation and glacial-interglacial changes which are still visible in sediment temperature profiles. Our results for the western Black Sea sub-basin in general confirm this conclusion in terms of the lateral extent of the GHSZ. However, some specific slope locations seem to have thicker GHSZ due to non-steady-state P-T conditions in the region. Such geological locations usually manifest high sedimentation rates which lead to significantly lower and transient (i.e. not yet equilibrated) temperature gradients and therefore, have major effects on the GHSZ extent (Riedel et al., 2021a, 2021b; Zander et al., 2017).

The total amount of gas hydrate for the present-day is estimated at ~14,607 Mt of carbon which is equivalent to ~139,884 Mt of gas hydrate and ~30,073 × 10¹¹ m³ of CH₄ at STP conditions (see Table 3). The surface of our model amounts to 139,855.66 km² and therefore,

leads to a gas hydrate resource density of ~0.104 MtC/km² (~0.215 billion cubic meters (BCM) of CH₄/km²). Gas hydrate estimates provided in Table 3 were calculated using dynamic space and time-dependent values of porosity, effective permeability, predicted gas hydrate saturation etc. calculated separately for each grid cell of the modeled sediments. According to the model predictions, a significant part of gas hydrate inventory is located close to the base of the predicted transient GHSZ which oscillates in depth between ~860 and ~520 mbsf in the central, deepest part of the sub-basin to roughly 30–40 mbsf in the shelf regions and even locally outcropping at the seafloor in the Romanian sector. Hydrate-bearing sands, mostly associated with deep-sea fan sedimentary facies, represent 38% of all predicted gas hydrate deposits. Gas hydrate accumulations in the central, predominantly shaly part of the basin account for 37%, while the remaining 25% is associated with mixed shale, marly-shale, and turbidite lithological facies. However, when considering the proportional volume of each sediment type present in the model, the highest resource density of potential economic interest is found in the coarse, sandy deposits from the Upper Miocene to the Holocene.

In the previous study of Burwicz et al. (2017), the importance of both methane sources in gas hydrate formation was studied in two independent scenarios where only biogenic and, consequently, only thermogenic methane formation was modeled. However, large disproportion of the biogenic vs. thermogenic gas hydrate accumulations (e.g. the case of the Black Sea basin) might lead to misinterpretations of such modeling results. Namely, in the absence of significant amounts of biogenic methane in the modeling domain, previously formed thermogenic methane accumulations might remain immobile and trapped outside the GHSZ. Due to the model restrictions, initially thermogenic gas hydrate deposits affected by dissolution or decomposition processes will be solely accounted for as a bulk hydrate volume. According to our results, only an extremely small fraction (i.e. about 1%) of all gas hydrate accumulations predicted by the model is initially of pure thermogenic origin. Gas hydrate accumulations consist almost exclusively of biogenic or recycled methane which is consistent with previous regional reports. This significant proportion of the biogenic methane component is directly related to favorable conditions of organic matter degradation in the basin, as well as with the apparent thermally immature state of the main organic-rich source rock—the Maykopian facies (Burwicz and Haeckel, 2020).

Present-day and past distribution and saturation of gas hydrates on a basin-scale is presented in Fig. 4 with highlighted regions of interests which were used to validate our model results (i.e. the Danube and Dniepr fan areas, as well as four gas hydrate provinces offshore Turkey, see Fig. 1). The region of the central Black Sea basin is located partially

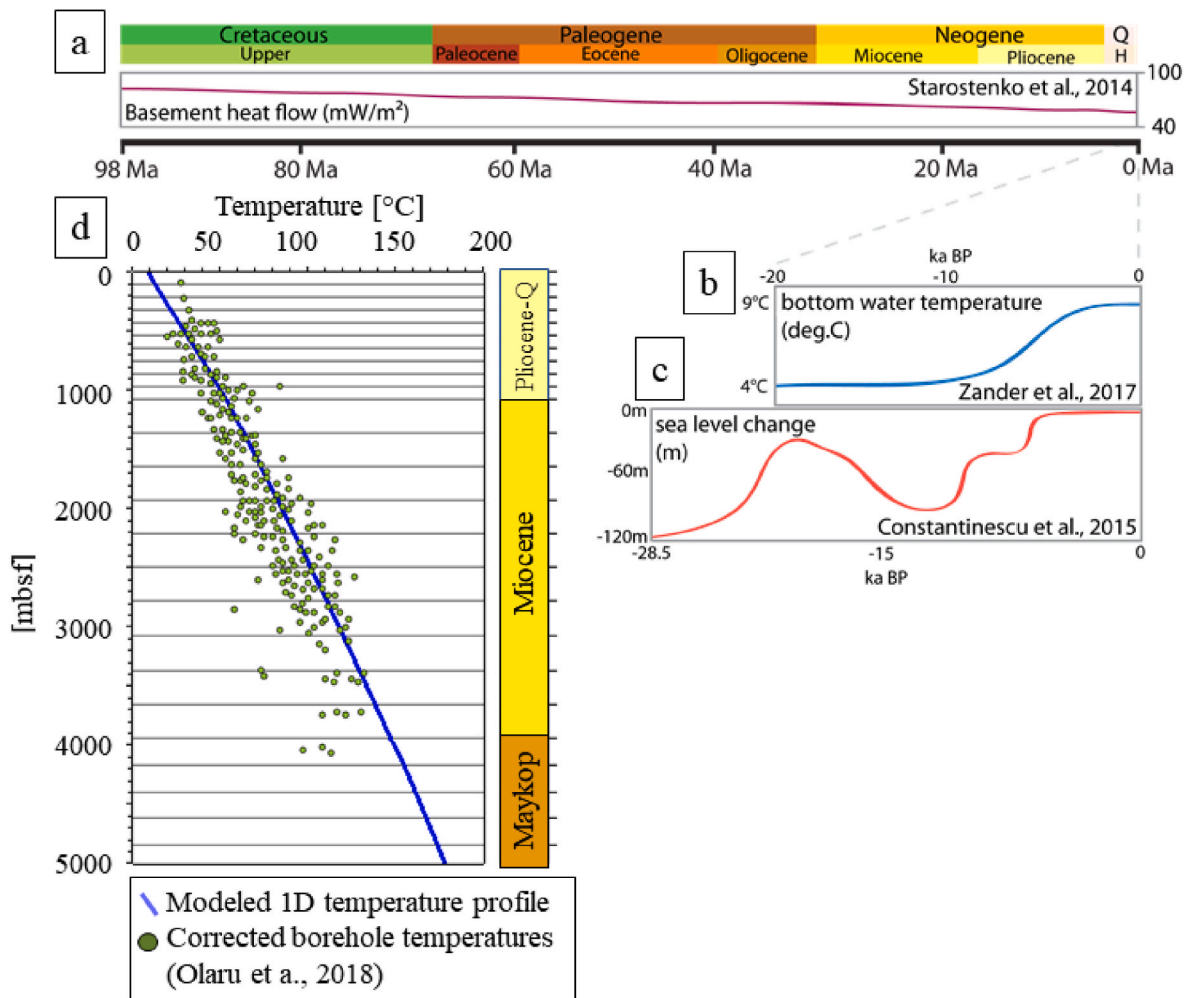


Fig. 3. Time-dependent boundary conditions used in the model (98 Ma–0 Ma) modified after Burwicz and Haeckel (2020): a) basement heat flow based on Starostenko et al. (2014), b) bottom water temperature changes based on Zander et al. (2017), c) sea level changes based on Constantinescu et al. (2015); d) modeled 1D temperature depth profile plotted against corrected borehole temperature measurements from Olaru et al. (2018).

Table 3

Present-day gas hydrate inventory predicted in the model.

Age of sediments (Ma)	Mt CH ₄	MtC	Mt of GH	m ³ CH ₄ (at STP ^a)
Holocene and Late Pleistocene 0–0.02	15,477	9,843	94,264	20,266 × 10 ¹¹
Late Pleistocene 0.02–0.04	3,411	2,170	20,777	4,466 × 10 ¹¹
Late Pleistocene 0.04–0.12	2,698	1,716	16,436	3,533 × 10 ¹¹
Middle Pleistocene 0.12–0.21	1,379	877	8,398	1,806 × 10 ¹¹
Middle Pleistocene 0.21–0.48	1.49	0.95	9.08	1.95 × 10 ¹¹
Total	22,967	14,607	139,884	30,073 × 10¹¹

^a Standard temperature and pressure (STP) refers to the nominal conditions of 15.556 °C and 101.325 kPa of pressure (Hantschel and Kauerauf, 2009).

outside of our model domain; therefore, we analyze it in less detail and focus on the most probable migration paths delivering methane to the remaining regional systems.

On the basin-scale, gas hydrate deposits show a large range of saturations as well as driving formation mechanisms at different parts of the basin. Generally, we identify moderate to relatively high (60–85 vol %) gas hydrate saturations located alongside the paleo-deep sea fan deposits (e.g. Danube, Dniepr, and partially Dniestr regions). These spatially focused hydrate deposits are usually attributed to the high lithological contact between highly permeable paleo channel deposits and less permeable surrounding sediments. This interpretation highlights the importance of long-distance methane transport as a main driver for gas hydrate formation of that type and is further analyzed in

detail in the next, regional sections of the paper. In contrast, significant, wide-spread gas hydrate deposits of moderate saturations (typically between 30 and 40 vol %) are present in the Bulgarian and Turkish Black Sea sectors. The pattern of such hydrate distribution seems to be different and related to the local basin geometry that favors intense regional gas hydrate recycling process previously investigated in other high sedimentation regimes such as the Green Canyon, Gulf of Mexico (Burwicz et al., 2017). Therefore, the main factors regionally differentiating the two end-member types of hydrate formation are the degree of sediment heterogeneity, the overall spatial position of sedimentary layers, the steepness of the slope, and the presence of regional plateau-like structures above the base of the GHSZ favoring gas hydrate recycling and the development of wide-spread hydrate deposits. The

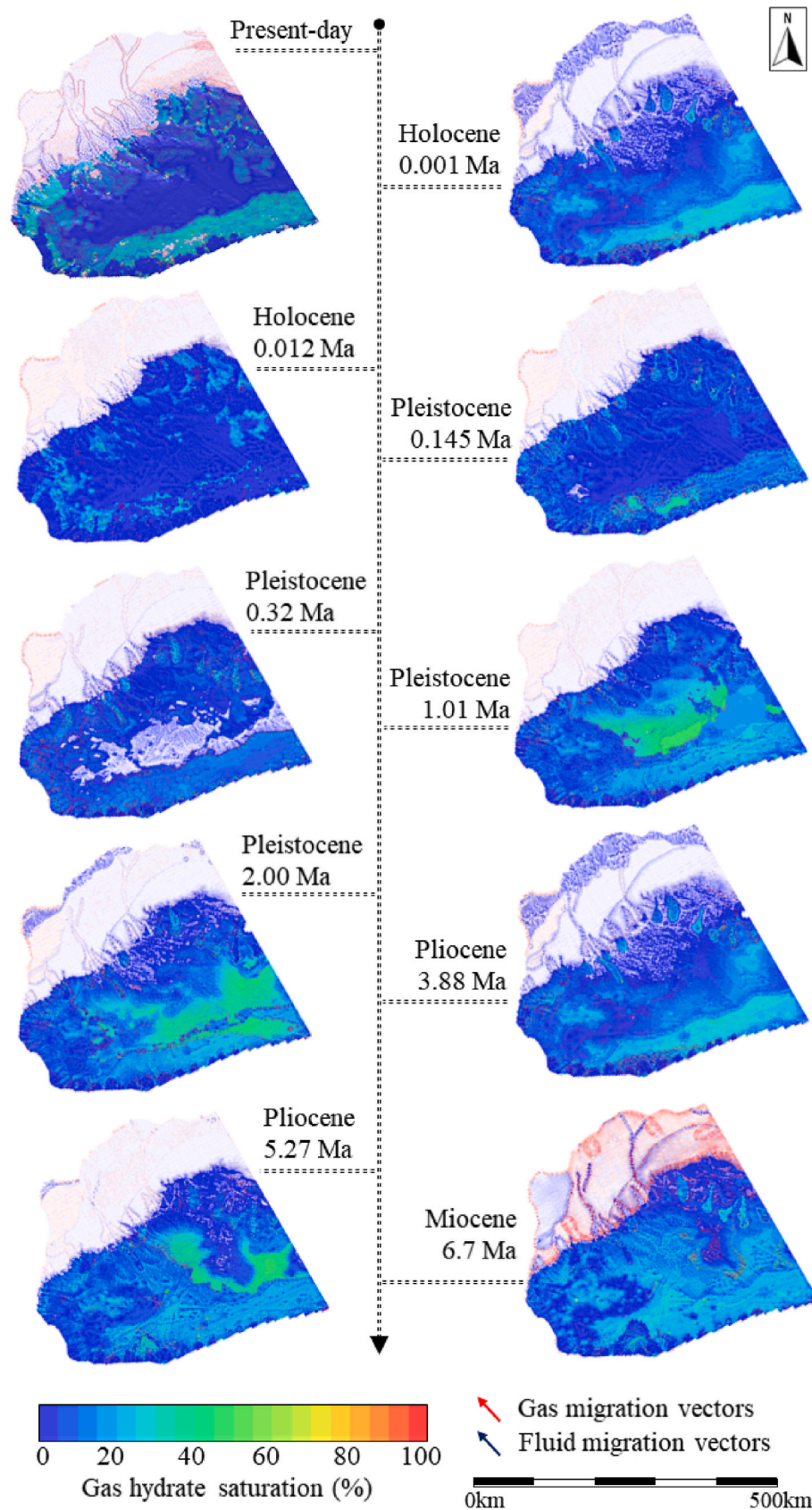


Fig. 4. Development of gas hydrate deposits in the western Black Sea basin presented as time-snapshots from late Miocene (6.7 Ma), Pliocene (5.27 Ma and 3.88 Ma), Pleistocene (2.00 Ma, 1.01 Ma, 0.32 Ma, and 0.145 Ma), Holocene (12 ka and 1 ka) until the present-day. Red and blue arrows represent the main gas and fluid migration pathways, respectively. Please note: only gas hydrate deposits with saturations above 1 vol % are plotted here.

other interesting finding is the lack of major gas hydrate-bearing sites (gas hydrate saturations less than 5 vol %, see Fig. 4) in the deeper part of the basin, i.e. beyond the outer shelf areas. This observation was previously made by Popescu et al. (2007) who attributed it to the fact that the near-shore locations act as methane accumulation areas whereas the deeper parts act as the methane sinks (Reeburgh et al., 1991). Our interpretation, which is based on the understanding of methane migration pathways from the past up to the present-day, is that the majority of biogenic methane generation occurs in-situ at shallower water depths. The deep-sourced biogenic methane in the central parts of the basin was, however, generated at larger scale, but has either been effectively transported towards the shore or escaped through the seafloor. Burwicz and Haeckel (2020) showed that the cumulative outflow of methane through the basin top for the entire western Black Sea basin ranges up to ~2,800 GtC of biogenic and ~800 GtC of thermogenic methane from the moment of generation up to the present-day with the main migration peaks during the late Paleogene. The latter might partially explain relatively small amounts of mobile thermogenic gas left to migrate towards shallower basin parts. However, significant gas hydrate accumulations with saturations commonly above 30 vol % and up to 60 vol % were present in the period from 6.7 Ma to about 1 Ma ago (Late Miocene – Pleistocene) as depicted in Fig. 4.

To understand these intriguing results, we have analyzed the development and spread of the gas and fluid migration pathways in the basin's past. The southern rim of the western Black Sea sub-basin seems to be relatively stable in terms of gas hydrate accumulations until the end of the Holocene when significant changes related to the sea-level fluctuations re-shaped the conditions for gas hydrate stability in this region causing several stages of repetitive dissociation and formation of hydrates. Previously stable hydrate deposits with mean saturations of 25–30 vol % were, on average, reduced to patchier and less dense accumulations (most likely about 15 vol %) in the period from 150 ka to 10 ka. After that time, a progressive re-growth of hydrate deposits in the southern part of the basin was observed as a result of, firstly, efficient in-situ methane generation and, secondly, gas hydrate recycling at the base of the GHSZ which shows its full characteristic in this region by forming wide-spread, relatively uniform hydrate saturations within the deposits.

A significantly different behavior is observed for the central basin hydrates of moderate to high saturations (~60 vol %) which remained stable until the late Pleistocene and then, consequently, dissociated, followed by methane migration towards the north-west parts of the basin along migration pathways in up-dipping sedimentary beds. It could be assumed that the large portion of methane which originated from the central basin-hydrates cycled into the prominent and active deep-sea fan regions in the north-west shelf (i.e. Danube, Dniepr and Dniestr) to accelerate gas hydrate formation there. In contrast to the southern part, complex basin architecture in this area does not allow for simple gas hydrate recycling. Therefore, enhanced fluid and gas migration pathways (marked as blue and red arrows in Fig. 4, respectively) highlight the efficiency of methane gas to migrate towards and beyond the GHSZ. Generally, since the late Miocene, there were no major changes on the basin-scale extent of the GHSZ that would be visible as a direct shift of the GHSZ limits in the shallowest shelf areas. Instead, local changes of the upper boundary conditions in the most recent epoch related to multiple events of sea-level transgression and regression are visible on a regional scale as well as significant changes in sudden sediment erosion and deposition related to the development of the pronounced deep-sea channels. Detailed examination of the regional gas hydrate inventories and their fate is discussed in the following sections of this paper. We have investigated: 1) two well-studied deep-sea fan systems of the Dniepr and Danube region which are characterized by patchy moderate to high gas hydrate saturations that most likely developed from a mixed methane source generated in-situ and recycled from the deeper parts of the basin, 2) four sites offshore Turkey that were formed due to, partially, gas hydrate recycling as well as the long-distance methane migration, and 3) the central Black Sea basin which is

currently depleted in gas hydrates, but is characterized by abundant mud volcano activity and related tectonic faulting.

4.1.2. Regional inventories

1. Dniepr fan region

Indications for free gas migration and potential existence of gas hydrate deposits in the Dniepr paleo-delta are mostly based on multibeam, seismic, and hydro-acoustic examinations of the pockmark structures (Naudts et al., 2006, 2008). More than 600 gas seeps have been detected in the Dniepr paleo-fan only, at water depths ranging from 72 to 156 m (Naudts et al., 2006). Both, locations of the seeps and intensity of seepage have been attributed to the presence of the underlying free gas front that migrates gradually from the deeper parts of the basin towards the shelf where it reaches the highest methane concentrations. Naudts et al. (2006, 2008) focused their observations on the central part of a pockmark field (i.e. on the outer shelf) characterized by water depths of about 105 m. Their observations suggest a direct link between the pockmark's NW-SE orientation at the seafloor and the morphology of the underlying paleo channels of the outer shelf filled with coarse-grained sediments. Moreover, these elongated and relatively large pockmark structures (up to 100 m wide and up to 500 m long) are thought to release significant amounts of biogenic methane: in comparison, 3 times more than the inner shelf area, and approximately 5 times more than the open basin. Furthermore, the authors compared the extent of the theoretical GHSZ with the location of the observed gas seepage (Naudts et al., 2006). According to the authors, major abundant methane venting sites seem to be located directly upslope and outside of the GHSZ limits, which corresponds to a water depth of about 665 m for a salinity of ~3 prevailing at 25–350 mbsf and a water depth of ~720 m for the bottom water salinity of 22.3, both for today's bottom water temperature of ~9 °C (Bialas and Haeckel, 2022). The extent of the GHSZ predicted by our model (Fig. 5) matches well with these values.

The existence of generally continuous BSRs in the region of the Dniepr delta has been reported by Lüdmann et al. (2004) within the depth ranges of about 700 to 1,350 mbsf. Beneath the apparent BSR, there is an indication for a prominent free gas occurrence zone coupled with a low-amplitude reflection zone directly above the BSR that suggests the presence of a ~100 m thick gas hydrate deposit. However, this interpretation is still debatable and should be treated with caution. Our simulation suggests a maximum thickness of the GHSZ in the region of about 830–690 m with local thinning to <150 m.

The gas hydrate inventory in the Dniepr paleo-delta region has been previously estimated at about $12 \times 10^{11} \text{ m}^3$ of methane or, equivalently, 0.6 GtC of methane (Lüdmann et al., 2004). These calculations were performed assuming a uniform gas hydrate saturation of 15 vol % within the deepest 100 m of the regional GHSZ. However, the results of our model suggest that the spatial distribution of gas hydrate deposits is not homogenous and varies considerably from the inner shelf towards the shelf break and further towards the open basin. Firstly, the distribution pattern of hydrate deposits seems to be much 'patchier' as presented in Fig. 5a. This 'patchiness' is related to the lithological contrasts between sedimentary facies and therefore, the efficiency of methane to migrate along the edges of sedimentary units. This relatively long- and medium-distance migration represents the advective transport component where methane dissolved in pore fluids as well as free methane gas are carried along the highest permeability pathways. The second component of methane transport, the diffusive migration, is driven by local gradients in methane concentrations and strongly depends on the effective diffusion coefficient, i.e. porosity, of the given lithology. The Dniepr delta area shows a good representation of both migration styles responsible for effective gas hydrate formation. Fig. 5b–c illustrates predicted gas hydrate saturations for cross-section A-B and modeled saturations of biogenic methane directly below the gas hydrate stability zone, respectively. Firstly, our results show the extent of the 'gas front'

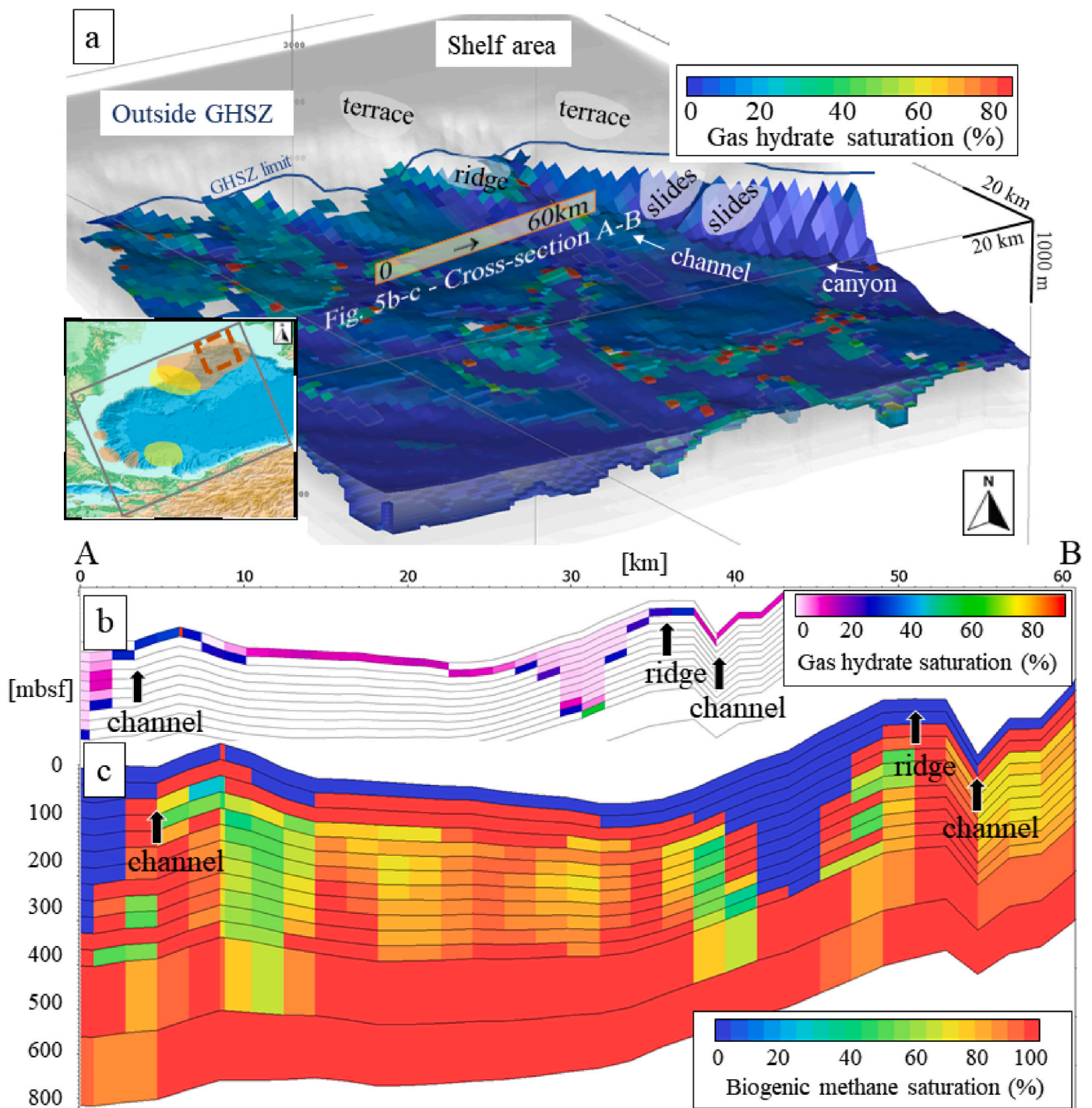


Fig. 5. A) Predicted present-day gas hydrate distribution in the Dniepr fan region. Cross-section A-B presenting: b) gas hydrate saturations, and c) biogenic methane saturation level in the pore space. All plotted cells are characterized by gas hydrate saturation of minimum 1 vol %.

represented by high biogenic gas saturations (>85 vol %) which correspond to the BSR depths and are formed as a result of an advective-diffusive methane transport towards the GHSZ. The shallowest depth of the gas front is located at local topographic highs (e.g. ridges on the flank of the channels) and directly links to the observations of Naudts et al. (2008). Moreover, our results confirm the observation by the same authors on the correlation of shallow gas front (below roughly 10 mbsf) with the existence of the seepage sites. Accordingly, gas hydrate saturations predicted for the local topographic highs where the gas front is relatively shallow are the highest and vary around 30–35 vol %.

The specific geometry of the seafloor in the Black Sea areas intruded by the paleo-deltas is often characterized by multiple ridge-like structures associated with deep canyon-like incisions and relatively flat parallel sedimentary levee layers in between (see Fig. 5). This type of geometry naturally promotes advection-dominated methane migration towards the steep gradients whereas the flat parts of the basin rely on more diffusion-dominated methane input which results in a ‘patchy’ or mosaic-like gas hydrate distribution (see Fig. 5a). According to our predictions, flat parts of the gas hydrate system located within the outer part of the slope are typically characterized by hydrate saturations of no

more than 15–18 vol % and a small ability to develop seepage sites due to the small amount of a free gas as well as the lack of developed overpressures. The absence of sufficiently rapid fluid and gas migration may result in the self-clogging ability of the system by the formation of methane-derived authigenic carbonates (MDAC) which would support the hypothesis of Hovland (2002). According to our results, this process likely occurs in the flat-type regions between the paleo-channels where migration efficiency is lower. It is also supported by observations of the abundant bacterial mats which might represent the first stage of the self-clogging process (Greiner et al., 2010; Hovland, 2002; Naudts et al., 2008).

Similar to the outer shelf region where the GHSZ reaches a thickness of hundreds of meters, the migration pathways of methane in the inner shelf region of the Dniepr delta remain complex. The interplay between the advection- and diffusion-dominated transport results in distinct gas emission patterns (see Fig. 6). From a detailed analysis of the modeling results, we conclude the existence of three dominant styles of methane accumulations, and ultimately, release from the seafloor. Fig. 6 shows the abundance of mobile methane gas that is not locked in a gas hydrate structure (referred to as a ‘gas front’ in the previous section) as well as the location of three methane venting sites (here depicted as A, B, and C in Fig. 6) reported by Naudts et al. (2006). Typically, the most methane-rich regions are directly adjacent to the edge of the GHSZ (regions B and C in Fig. 6), especially in the case of steep topographical gradients, i.e. the sediment slides (region C in Fig. 6, see also Fig. 5 for location). Region C (Fig. 6) is an example of a location predominantly prone to host methane vent sites. The outcropping limits of the GHSZ provide sufficient conditions for advective-diffusive transport of methane towards the seafloor in an area that is 2–4 km away from the GHSZ edge towards the inner shelf. Distances towards the land larger than about 4 km are expected to be relatively depleted in methane (50–65 vol % CH₄ gas saturation) in comparison to the GHSZ edges (>90 vol % CH₄). Region B (Fig. 6, referred to as a ‘terrace’ and partially

a ‘ridge’ in Fig. 5) shares some characteristics with region C, however, due to the different geometry of the seabed and the underlying sedimentary layers, the amount of methane gas is slightly smaller (~85 vol %) and results in less gas venting. Both sites, B and C, are fueled mostly by the advective transport of gas alongside sedimentary units of different lithologies and by the premises of the GHSZ limits. However, a different mechanism drives the abundant but far less effective seepage sites in the region A (Fig. 6) which is located closest to the shore line and therefore, furthest away from the GHSZ and prominent channel-like structures. This region is characterized by the highest saturations with biogenic gas (>85 vol %), however, mostly diffusion-dominated or slow advective transport results in a rather slow and progressive venting regime compared to the more dynamic counterparts closer to the outer shelf. Overall, the complex local geometry of the basin seems to have the largest control over methane discharge styles and either promotes or diminishes the ability of methane to escape through the seafloor.

Finally, we have conducted a detailed analysis of the development of methane migration patterns in the basin’s past. Strikingly, we observe a clear time-related pattern of the seep development from the inner to the outer-most parts of the Black Sea shelf in the Dniepr area. Seepage sites associated with slow, perhaps periodic, advective transport located in the inner part of the shelf have been active for much longer (~320 ka; region A in Fig. 6) than the seeps located towards the outer shelf (~26.5–30 ka; regions B and C in Fig. 6) and beyond. Locally developed seepage sites driven by the advective gas transport in the deepest parts of the shelf are most-likely associated with the free methane gas migration through the GHSZ due to preferential topographic conditions (i.e. local heights) and shallow gas front depths. Such structures modeled for the Dniepr paleo-delta region are representing the youngest methane escape structures on the regional scale (~13.2 ka) and most likely reflect the most recent fluctuations in the GHSZ thickness for the past glacial-interglacial periods.

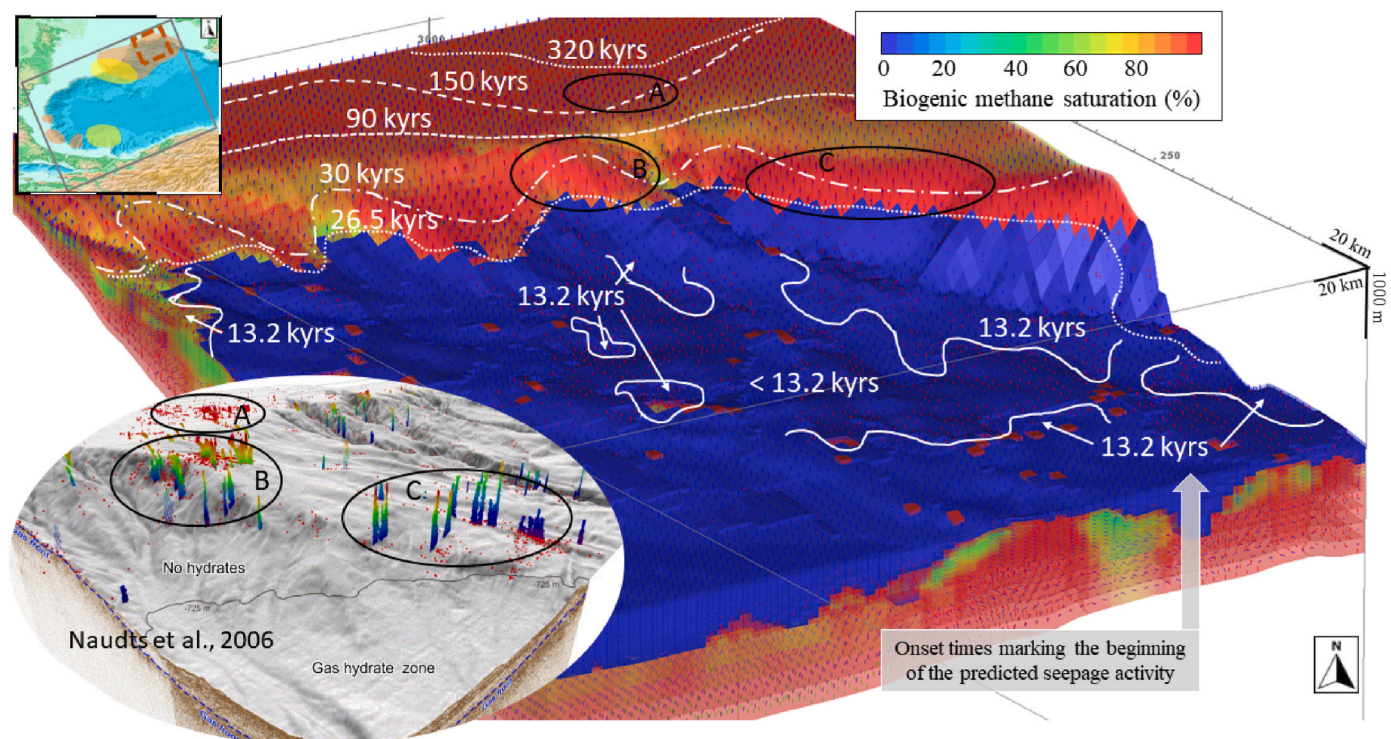


Fig. 6. Saturation of biogenic methane in the present-day deposits in the Dniepr region. Saturation values (in percent) indicate the amount of a pore space occupied by biogenic methane. The lower insert shows the location of methane seepage sites reported by Naudts et al. (2006). Regions in blue indicate model cells in which biogenic methane is bound in gas hydrate.

2. Danube fan region

Similar to other regions in the world where complex burial history and boundary condition fluctuations create transient GHSZ states (Burwicz and Rupke, 2019; Grevemeyer and Villinger, 2001; Phrampus

et al., 2014; Plaza-Faverola et al., 2017), the Danube delta region presents a challenge in characterizing this natural gas hydrate system and its complexity. Present-day GHSZ thickness in the northern part of the Danube delta stretches from the seafloor, close to the shelf area, up to ~500 mbsf, corresponding to water depths of ~660–720 m towards the

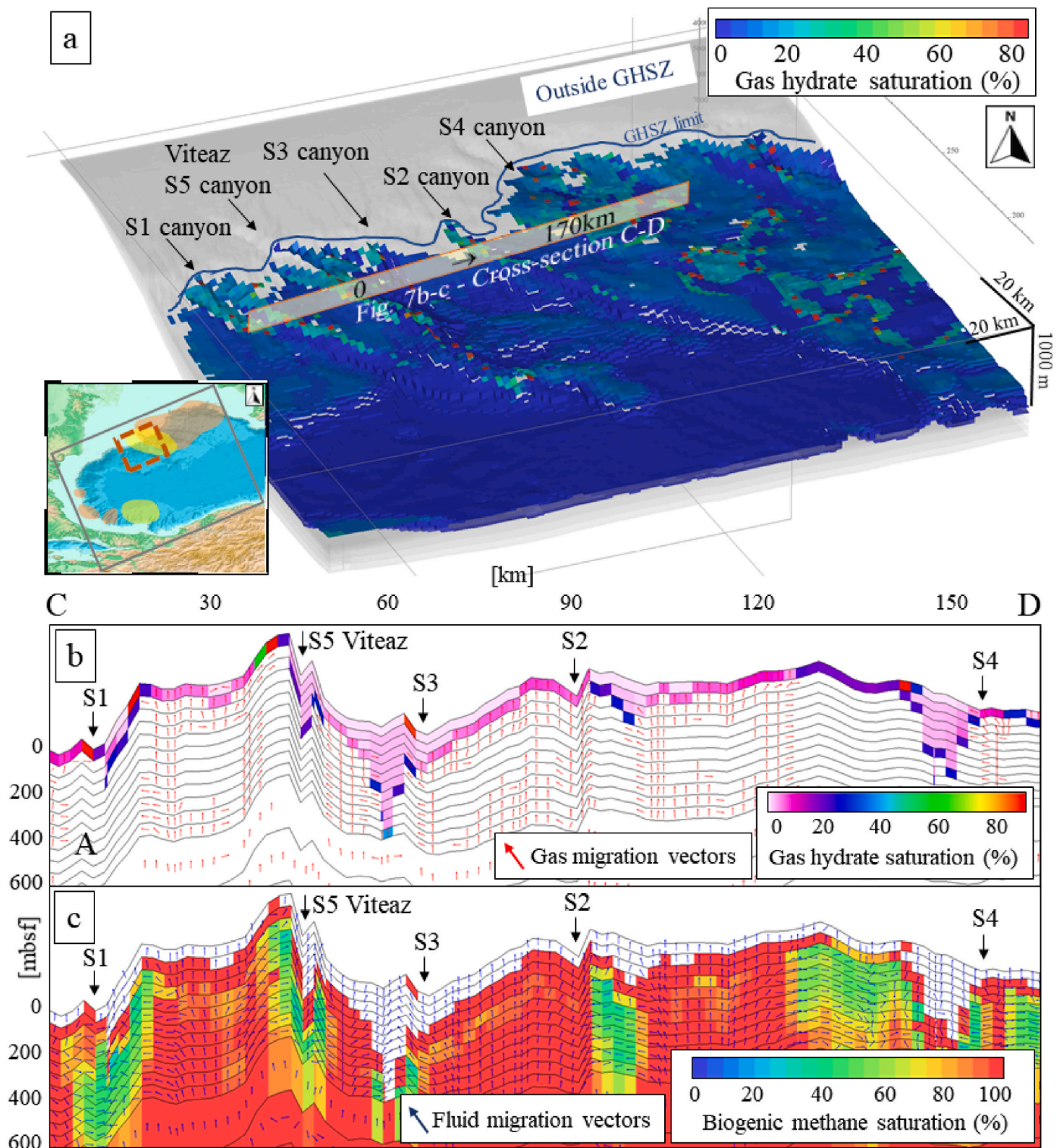


Fig. 7. A) Gas hydrate saturations in the Danube delta region with the locations of investigated sites: S1-S5 canyons, including the main Danube channel (i.e. the S5 Viteaz canyon), b) cross-section C-D presenting gas hydrate saturations larger or equal 1 vol %, and c) methane saturation level in the pore space in the Danube fan region. Gas and fluid migration vectors, respectively in red and blue, highlight the main pathways of methane transport across the channel units. The uppermost part of the sediment column with enhanced methane gas saturations (c) can be interpreted as a ‘gas front’ below the GHSZ. Transparent cells in the lower plot mark the locations where methane is trapped in a form of gas hydrate and thus, becomes immobile.

open basin. These predictions correspond well with abundant methane seepage areas around such water depths (Ker et al., 2019; Riboulot et al., 2017). However, the complex geological history of the region has significantly modified the main environmental parameters controlling the GHSZ, such as the sea-level stand, pore water salinity, and geothermal gradient. Particularly, the Danube region is known for the occurrence of rare phenomena of multiple BSRs (see Fig. 1 for the exact location), which highlights the transient conditions in the past and at present-day both in the western (Colin et al., 2020; Hillman et al., 2018a; Popescu et al., 2006; Zander et al., 2017) as well as the eastern Black Sea (Monteleone et al., 2024). The formation of multi-BSR systems in the Danube delta was explored previously and is likely caused by rapid sedimentation events of the levees of the paleo-Danube system at sea-level low-stands. Gupta et al. (2024) and Zander et al. (2017) showed that free gas and gas hydrates at former BSRs in the Danube paleo-delta can survive over time-spans of ~300 ka. Recently, Riedel et al. (2021b) reported on a new set of previously not recognized seismic reflections from the Danube delta (S2/S4 channels, see Fig. 7 for location details) which might represent the most recent BSR conditions. Due to its discontinuous character, the BSR might be related to the presence of locally existing methane pathways which either break the seal of formerly crystallized gas hydrates or use currently hydrate-free sediments to migrate upwards from underlying layers. Our modeling study does not track the development of multiple BSRs in the subseafloor, however, it considers transient P-T-S conditions during sediment deposition and erosion events. Our simulations resolve non-steady-state conditions of the gas hydrate system governed by changes in the upper boundary conditions (i.e. sea level, bottom water temperature, water salinity) coupled with ‘thermal-blanketing’ effects caused by rapid deposition of large amounts of clastic material (i.e. formation of channel-levee systems). Therefore, presented BSR depths and the spatial extent of the GHSZ are representative for present-day conditions, which are not at full steady-state in the Black Sea, allowing for model calibration and comparisons with direct regional observations.

Gas, pore water, and gas hydrate samples collected from the Danube delta region suggest that the large majority of hydrate-forming gas is methane (>99.5 mol %) with small additions of nitrogen and carbon dioxide (Chazallon et al., 2021). The results of isotopic composition analysis clearly indicate the microbial source of methane that was generated from carbon dioxide reduction (Chazallon et al., 2021; Pape et al., 2020; Zander et al., 2020). Following these findings, GHSZ calculations in the model are performed for structure I pure methane hydrates. According to our simulations, more than 99% of all hydrate deposits in the Danube delta region are of biogenic methane origin which is consistent with the present-day understanding of this natural gas hydrate system (Popescu et al., 2007).

Gassner et al. (2019) estimated gas hydrate saturation in the S1 channel area investigated during the MSM 34-2 cruise in the south-western part of the Danube delta region (see Fig. 7) at roughly up to 25–28 vol % and free gas saturations of about 1.2 vol % based on the seismic inversion method. However, derived gas hydrate and methane gas concentrations at the BSR level are locally patchy and do not form a continuous layer. Another gas hydrate estimate based on the data obtained with the CSEM method (controlled-source electromagnetics) suggests gas hydrate saturations of about 10 vol % in the channel fills of the ‘SUGAR’ S1 channel region (Schwalenberg et al., 2020). Higher predictions were made for the channel ridges and levees amounting to about 20–23 vol %, unlikely to the channel S2 area where no gas hydrates or saturations below 10 vol % are indicated with possible small amounts of a free gas present at the BSR depth (Duan et al., 2021; Schwalenberg et al., 2020). The authors relate these discrepancies to the fact that both sites are located at different water depths (S1 channel at ~1,560–1,620 m, S2 channel at ~1,770–1,900 m) and are most likely charged from different methane sources. Gas hydrate saturation derived from P-wave anomalies in the S1 channel lead to similar values of 6–30 vol % and the free gas locally of up to 40 vol % (Bialas et al., 2020).

Gas hydrate concentrations derived from our modelling are largely consistent with these geophysical estimates (Fig. 8 for a regional

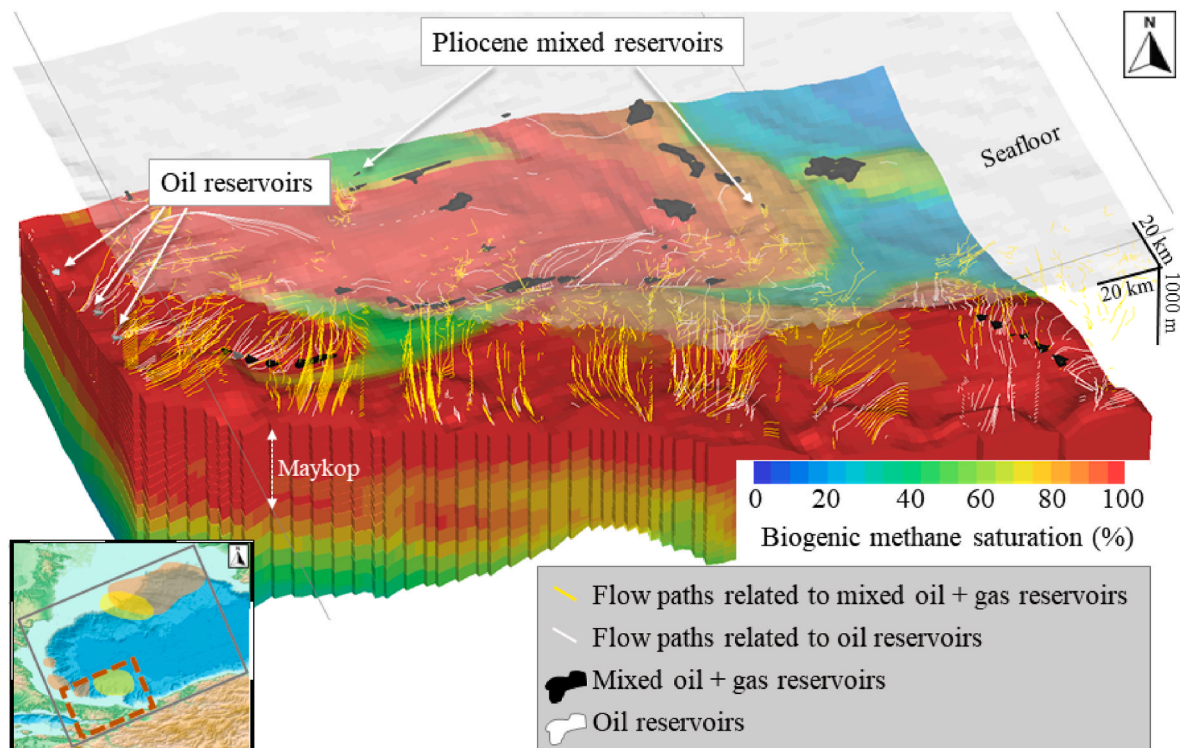


Fig. 8. Regional model of the biogenic methane saturation in the sediments offshore Turkey. Plotted are the layers from Cretaceous basement (98 Ma) up to the Maykopian age (late Eocene-early Oligocene) to highlight the location of oil (white) and mixed-oil and gas reservoirs (black). All predicted reservoirs are located within the upper Maykopian layers, besides two mixed Pliocene reservoirs accumulated in the layers deposited ~13 ka ago.

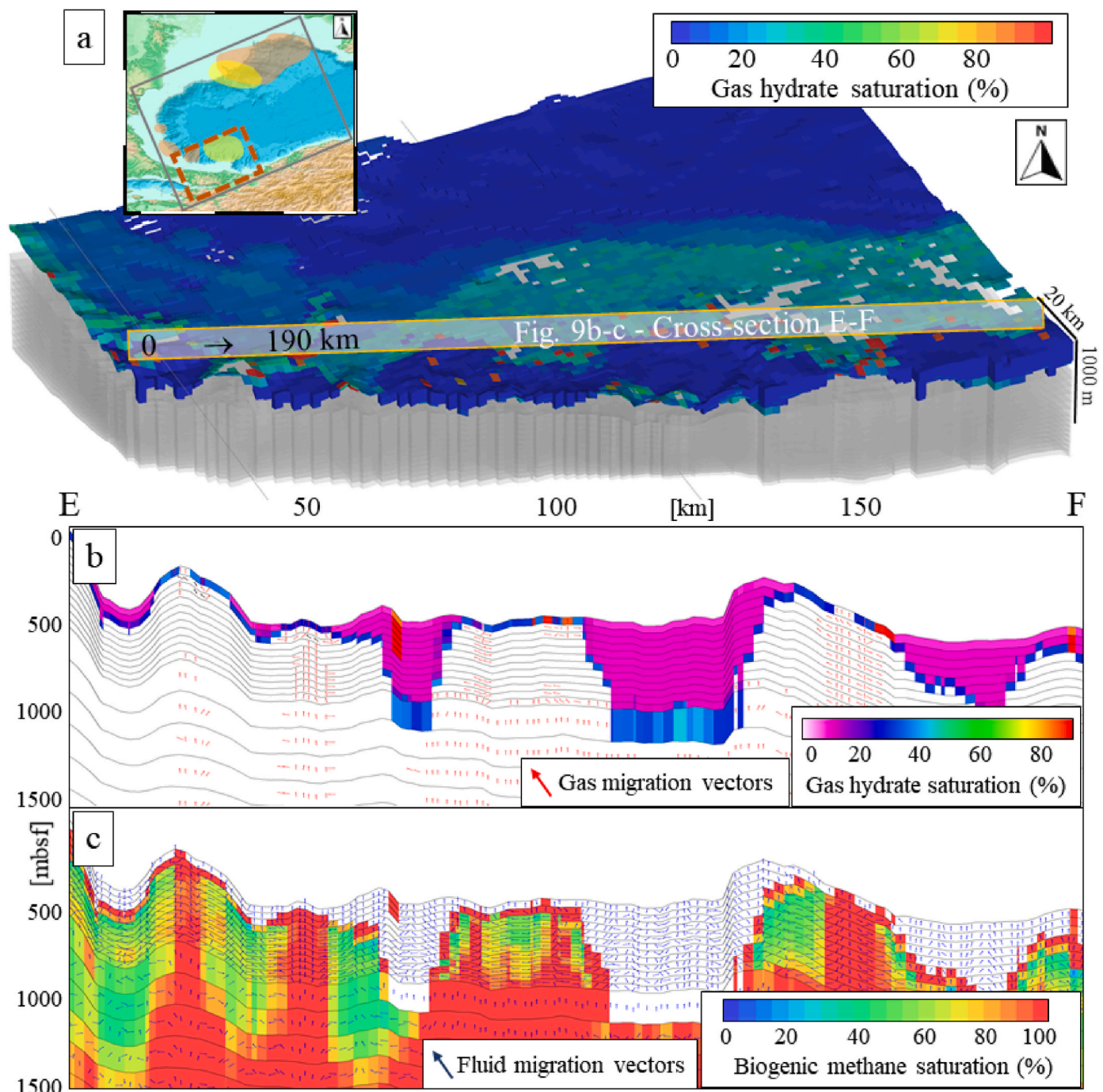


Fig. 9. A) Gas hydrate distribution offshore Turkey, b) Cross-section E-F presenting gas hydrate saturations larger or equal 1 vol %, and c) methane saturation level in the pore space offshore Turkey. Gas and fluid migration vectors are illustrated in red and blue, respectively.

estimate and Fig. 9a for a cross-section comparison). Typical background gas hydrate saturations for the Danube region range around 10–15 vol %, locally up to 25–30 vol %. Rarely, very high hydrate saturations (60–85 vol %) were predicted for single model cells where the combination of parameters driving gas hydrate formation was unique; high methane supply from multiple directions coupled with preferential slope geometry favoring rich gas hydrate accumulations. We envision that such local, highly heterogenous conditions might in fact exist in the specific setting of paleo-deep water fans in the Black Sea, such as the Dniepr or Danube deltas although proving the evidence for such hydrate ‘hot spots’ might be challenging.

Our analysis of the gas hydrate concentration patterns coupled with methane migration towards the GHSZ shows two intriguing hydrate formation styles in the region. Firstly, moderate hydrate saturation of 15–25 vol % are commonly predicted for the deeper GHSZ parts and in between the channels (see Fig. 7b) where there is a direct contact between the GHSZ base and the free methane gas supply. Such gas hydrate enrichment close to the GHSZ base is most likely responsible for widespread BSR occurrences in the region and is directly related to a non-limited methane supply from the underlying layers with both advective and diffusive components which can be derived from the presented methane migration vectors in both fluid and gaseous form (see Fig. 7b–c,

red and blue arrows indicating flow directions and intensity). We can observe both gas hydrate recycling at the base of GHSZ, and direct incorporation of largely in-situ-formed methane into gas hydrate deposits. It is consistent with the interpretation of Popescu et al. (2007) who report on free methane gas being immediately trapped by gas hydrate as it enters the GHSZ. Our results are also supporting the hypothesis of Popescu et al. (2007) on gas hydrate acting like a physical flow-limiting buffer that restricts the access towards shallower parts of the GHSZ. Secondly, we made observations on the intriguing mechanism of 'by-passing' the base of the GHSZ (which usually effectively traps upward migrating methane) and developing an alternative migration path. Such effective migration mechanisms develop if local lithology and layer geometry allow for the formation of vertical escape structures with increased permeability, e.g. seismic pipes or chimneys (Liu et al., 2019), or upward dipping permeable river channel fills, such as the S5 Viteaz canyon or the slope of the S1/S3 channels (see Fig. 7). This alternative migration style is also reflected in reduced biogenic methane saturation directly beneath the exceptionally high gas hydrate saturations (see Fig. 7b–c) implying that the most effective methane migration charging gas hydrate 'hot spots must occur via different pathways. In this case, sources of methane are not restricted to the in-situ formed reservoirs, but rather require a secondary supply source. We suggest that such an additional source could be located towards the open basin and potentially include deep biogenic gas that would be transported over a much longer distance. Significant paleo-channel structures in the region would, therefore, successfully prevent methane from being trapped in a form of gas hydrate close to the BSR depth.

Additionally, the regions within S2/S4 channels where the newest and, at the same time, shallowest BSRs have been reported (Riedel et al., 2021b), show a significant enhancement in migration rates directly beneath the incisions of both channels which is not a common phenomenon in case of the other canyons. In comparison, gas hydrate deposits from the Viteaz canyon seems to be charged from a different, horizontally migrating methane source (see Fig. 7 for comparison). These results are in good agreement with the hypothesis of Riedel et al. (2021b) who attribute the development of new shallow BSRs to a vertical, rather than a lateral, gas migration.

The existence of large mass transport deposits (MTDs) in the Danube region, most likely caused or at least significantly contributed to the development of the methane seepage sites on the flanks of the canyon deposits, for example in the S2 and S4 channels (Bialas et al., 2020; Hillman et al., 2018b; Riedel et al., 2021c). Gas migration pathways in the region of the Danube delta analyzed in detail by Hillman et al. (2018b) revealed that slope failure features, such as sediment slumps in the area of the S2 channel, correlate with abundant methane seepage. This observation based on seismic data is supported by our modeling results on relatively short-distance methane transport on the flanks of S2 channel due to abundant methane reservoirs in shallow sediments which could be easily re-mobilized by slope failure events and sediment re-organization (see Fig. 7). Methane gas supply responsible for gas hydrate formation in the S1 channel region is most likely transported horizontally along the carrier beds or BSR due to insufficient migration patterns predicted directly below the channel (see Fig. 7a). These results stay in agreement with observations made by Bialas et al. (2020) who reported no vertical fluid or gas migration structures in the region.

Overall, the significant effect of geomorphology on methane migration in the Danube delta fan is somewhat similar to the Dniepr delta. The most prominent long-distance migration pathways with advection-dominated transport are predicted alongside the main sedimentary units e.g. paleo-channels and directly below the gas hydrate stability zone which is most likely related to the ability of gas hydrate to partially seal the pore space and reduce sediment permeability. Short-distance methane migration is predicted for the regions associated with mass transport deposits (MTD) and sediment slumps which facilitate the development or re-opening of more permeable transport pathways. According to our simulations, the erosional history of the region related

to the formation of submarine canyons contributed to gas hydrate destabilization and methane migration on a distance of up to a few kilometers, which could be considered as a third, mid-distance, type of migration pathway.

3. Offshore Turkey

The Black Sea region offshore Turkey is well-known for its abundant slide and slump structures, large number of canyons, buried debris flows, and the existence of small-scale normal faults, and scarps (Dondurur et al., 2013). It is characterized by a narrow shelf area (~3 km) and a steep shelf break at water depths of about 120 m (Dondurur et al., 2013). Triggering mechanisms of the submarine landslide development are still under discussion and include e.g. seismic activity and gas hydrate dissociation related to sea-level changes. The origin of gas hydrate present in this region is not known, however, the neighboring commercial oil and gas reservoirs suggest the potential of thermogenic gas hydrates. In this study, we analyze the region of the Sakarya canyon-offshore Akçakoca-Zonguldak-Amasra (see Fig. 1 for detailed location) to understand the mechanisms of gas hydrate formation and development of associated migration pathways.

Özel et al. (2022) reported a number of gas chimneys, seafloor gas flares, and mud volcanos located mostly in the outer part of the slope and towards the open basin. Based on the acoustic data, multiple gas accumulations were identified by the two types of BSR reflections in the large portion of the region for water depths between 750 and 1,950 m (Nasif et al., 2020). These two types of BSRs are often correlated with the existence of both biogenic and thermogenic gas accumulations, and therefore a potentially mixed gas hydrate source (Nasif et al., 2020; Özel et al., 2022). However, to our knowledge no direct hydrate sampling data was publicly shared until to date. Based on our results, we confirm the possibility of adequate gas accumulations of thermogenic source in the region that will be sufficient to charge shallow gas and gas hydrate systems offshore Turkey as well as the mud volcano structures (see Fig. 8). Significant migration pathways of both, oil but mostly gas components in the south-north direction are simulated by our model and illustrated in Fig. 8 with white and yellow lines, respectively. Similar to the other locations in the Black Sea where local basin geometry is dominated by the development of channel-like erosional structures, the migration pathways offshore Turkey seem to be largely controlled by the geomorphology of the region. Interestingly, one of the two predicted Pliocene sand reservoirs corresponds well with the location of the new Sakarya gas field which remains to be the largest commercial discovery in the Black Sea at a water depth of over 2,000 m (Aydin and Mery, 2021).

No quantitative gas hydrate predictions based on the seismic data have been made for this region so far. Aydin and Mery (2021) used a value of 50 vol % gas hydrate saturation in the 50-m thick sand layer to calculate the theoretical production tests from the field located next to the Sakarya gas site. According to our modeling results illustrated in Fig. 9, gas hydrate deposits are most likely contained within relatively narrow band outlined by the shelf break with mean saturation of ~25 vol %. There seems to be a relatively drastic transition towards low- or non-hydrate settings towards the open basin, firstly, indicated by a reduction of hydrate saturation to 8–10 vol % and rapidly to ~1 vol %. However, moderate saturations closer to the shore are rather homogeneous with local variations up to 32 vol % and uniform distribution within the sediments which suggest a large component of gas hydrate recycling as a driving force of development.

Interestingly, multiple patches of high hydrate saturation (>80 vol %) are visible in the vicinity of the canyon structures. In the other Black Sea regions, we interpret such gas hydrate distribution as a result of a local seabed morphology that favors gas migration towards topographical heights and contributes to the formation of chimney-like structures. However, in the Turkish sector of the western Black Sea, high saturation gas hydrate predictions are rather more clustered and coincide with the

predicted thermogenic methane migration pathways (see Fig. 8) which suggests atypical for the Black Sea enrichment in thermogenic hydrates. A typical shape of the shallow gas front in underlying GHSZ sediments illustrated in Fig. 9b–c is in good agreement with interpretations from Özel et al. (2022) based on seismic data.

The analyzed sediment cross-section E-F (Fig. 9b–c) shows the extent and the level of gas hydrate saturation (Fig. 9b) alongside biogenic methane saturation (Fig. 9c). In general, biogenic methane contribution is on a similar level or slightly lower than in the other Black Sea provinces analyzed by us, however, gas hydrate saturations seem to be higher. Interestingly, vertical transport of hydrocarbons towards the GHSZ seems to play an important role in overall gas hydrate distribution. It could be attributed to the fact that the sharp shelf break and the resulting high slope steepness in the Turkish Black Sea sector are additionally promoting methane migration from greater depths.

4. Central Black Sea region

The central Black Sea region (south of the Crimean Peninsula) known for multiple mud volcano occurrences (Kruglyakova et al., 2004; Xing and Spiess, 2015) is at least partially located within our model domain (see Fig. 1). Abundant seafloor expressions such as pockmarks, seepage sites, authigenic carbonates, and predominantly mud volcanos have been mapped and studied (Xing and Spiess, 2015). The regional history of sediment deposition is often dominated by two distinct sedimentation regimes. Firstly, a distant deposition of clastic coarse-grain material

from unchanneled fan formation of a paleo-Don river (north-east direction) in the late Pliocene-early Pleistocene ages, was followed by progressive deposition of massive paleo-Danube and paleo-Dniepr deposits about 900–800 ka ago from the western direction (Winguth et al., 2000) which was dominated by the sea-level low- and high-stands (Bahr et al., 2006). In our model, we do not explicitly resolve for the mud volcano formation, however, we provide evidence for the past and present-day conditions contributing to the development, such as methane saturation levels, geometry of the sediment packages and migration pathways.

Free gas and gas hydrate indicators, such as the BSRs, are generally absent in the region or located shallower than the estimated steady-state GHSZ which reflects the transient thermal conditions of the area, most likely related to the presence of mud volcano structures, which locally increase the geothermal gradient drastically. Accordingly, two out of six mud volcanos reported in the region are located within our model domain, i.e. the MSU and Yuzhmorgeologiya (Xing and Spiess, 2015) (see Fig. 10 for detailed location). The Yuzhmorgeologiya volcano, located directly in the eastern direction from MSU, experienced two major activity stages at ~905 ka and 43 ka ago. The MSU volcano was reported to show three major activity stages, ~900 ka, 140 ka, and 45 ka ago with the second and the third event occurring during the dominance of the paleo-Danube and paleo-Dniepr depositions (Xing and Spiess, 2015). Isotopic gas composition derived from this location suggests a mix of biogenic and thermogenic components (Ivanov et al., 1996). Xing and Spiess (2015) suggest that the biogenic component originates from

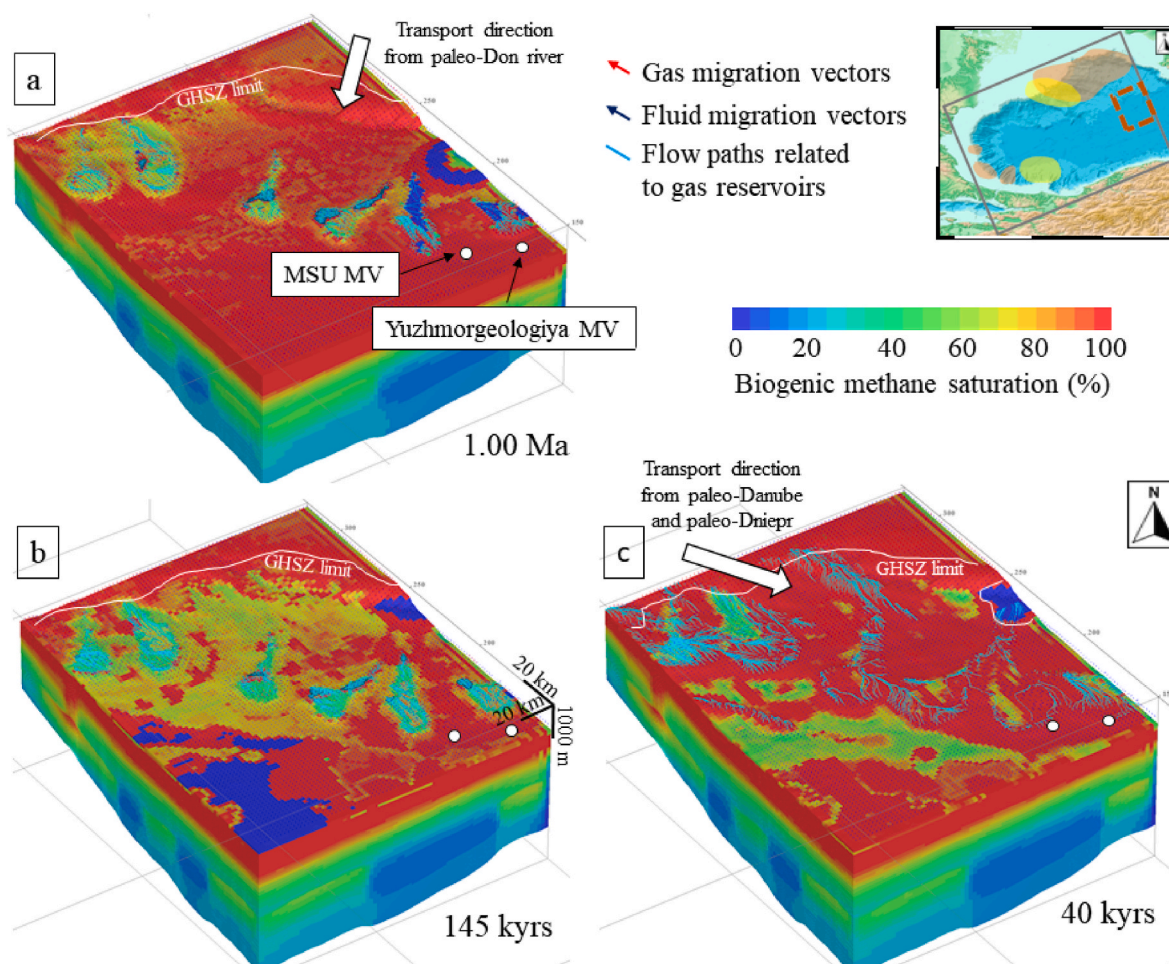


Fig. 10. Biogenic methane saturation levels in sediments below the GHSZ: a) 1 Ma ago, b) 145 ka ago, and c) 40 ka ago. Main transport directions of sedimentary material from the paleo-Don, Danube, and Dniepr rivers are indicated. The location of two mud volcanos (MV), MSU and Yuzhmorgeologiya, situated within the model domain is depicted with white circles. Gas reservoirs as well as the respective flow paths used for charging are highlighted in light blue color.

in-situ organic matter degradation or dissociation of neighboring gas hydrate deposits, whereas the thermogenic part most likely migrated through highly permeable feeder channel underneath the volcano, originating in the deeply-buried, organic-rich Maykopian formation (Dimitrov, 2002).

To analyze the origin of gas and development of the migration pathways on a broader-scale, we focused on three periods of basin formation that correspond to the activity stages of the MSU mud volcano, i.e. 1.00 Ma, 145 ka, and 40 ka ago according to the time resolution of our model (see Fig. 10). The sedimentation regime during the oldest period, i.e. 1 Ma ago is characterized by relatively flat and parallel to the sea-floor sediment deposition with an exception of the paleo-delta fans that bring more clastic material from the northern direction of the Crimean Peninsula. The examined area of the MSU and the Yuzhmoregeologiya mud volcanos is situated closely to the outer extent of the fan, therefore no significant erosional events occurred; the major Danube and Dniepr delta fans are still absent at this point. Interestingly, we predicted relatively large mixed biogenic-thermogenic gas reservoirs in the underlying Pliocene layers (see Fig. 10a). The ratio of biogenic to thermogenic components in these reservoirs is ~97.45:2.55 % which agrees with the analysis of local gas samples. Therefore, we can support the hypothesis of Xing and Spiess (2015) that large portions of deeply originated gas also from the Maykopian source rock migrated through or even co-developed the main mud volcano feeder channel and contributed to the potential overpressure development.

In contrast to the simulation results illustrating this geological setting 1 Ma ago where fully methane-saturated sediments dominated the entire region of interest, biogenic methane saturation levels 145 ka ago tend to be patchier and located predominantly in the deeper part of the basin and therefore, away from the outer shelf (see Fig. 10b). Although the extent of the paleo-Danube and paleo-Dniepr deltas lies outside the presented region of interest, their influence is already visible from analyzing fluid and gas migration vectors and on a broader-scale map (e.g. Fig. 4). We interpret this shift of biogenic methane saturation levels as a result of, firstly, progressive development of the paleo-Danube and paleo-Dniepr deep-sea fans which drained methane from the surrounding sediments and allowed for more efficient migration upslope, and, secondly, to the sea-level fluctuations related to glacial-interglacial periods which liberated large portions of methane from the regions adjacent to the GHSZ edge.

Visible shifts in sedimentation regimes can be observed in the model snapshot of 40 ka ago (see Fig. 10c). Major migration pathways as well as the charging paths for gas reservoirs changed from north and north-east to north-west and west reflecting the final stages of long-distance sedimentation of the Danube and Dniepr rivers. Another interesting aspect is the almost complete disappearance of the gas reservoirs present in the past. According to these results, we propose a scenario in which the previously formed mud volcano feeder channels served as pre-formed high permeability pathways facilitating gas and fluid flow from deeper layers since the amounts of over-pressured gas in the system do not seem to be sufficient to trigger the formation of new mud volcanos.

5. Conclusions

Gas hydrate inventories in the western Black Sea basin are predicted to 14,607 Mt of carbon, equivalent to ~139,884 Mt of gas hydrate and ~30,073 × 10¹¹ m³ of CH₄ at STP conditions. Considering the model surface of 139,855.66 km², the resulting gas hydrate resource density is ~0.104 MtC/km² (equivalent to ~0.215 billion cubic meters (BCM) of CH₄/km²), which suggests about 5 times higher gas hydrate concentrations in the western Black Sea basin, compared to the average gas hydrate density at continental margins (~0.02 MtC/km² after Burwicz et al. (2017)). In comparison to other basin-scale resource estimates

available in literature, these estimates are lower than the numbers reported for the major hydrate systems of the Green Canyon, Gulf of Mexico with a gas hydrate density of 1.56 billion cubic meters (BCM)/km² (Burwicz et al., 2017), or for the Terrebonne Basin of ~1.8 BCM/km² (Frye et al., 2012). However, the model domains of the two mentioned gas hydrate provinces in the Gulf of Mexico were strictly designed to cover the most prominent gas hydrate accumulation regions, whereas in our calculations, the total basin surface was considered which includes significantly lower gas hydrate saturations in the central part of the basin.

The gas hydrate distribution in the western Black Sea basin is complex and results from an interplay of parameters: rates of sedimentation throughout the basin history, local facies development and lithology contrasts, including the presence of the deep-sea fans and basin geometry. Sites of gas hydrate accumulations include: 1) large plateaus with moderate hydrate saturations (25–35 vol %) related to gas hydrate recycling, 2) localized chimney-like structures with high hydrate saturations (>80 vol %) related to the formation of high permeability pathways allowing efficient methane migration, and 3) paleo-river channel systems with typically steeper geomorphology enhancing advective methane transport by-passing the buffering zone close to the GHSZ base.

In-situ generated biogenic methane, especially in the inner shelf areas, seems to be the main contributor to abundant gas hydrate deposits of small to moderate saturations (10–20 vol % in case of the paleo-channels of e.g. the Danube and Dniepr; about 25–35 vol % in case of hydrate recycling zone in local plateaus e.g. southern-east or southern-western of the western Black Sea basin). Large contributions of deep biogenic methane towards the formation of gas hydrates are most likely possible due to large-distance migration pathways from the open basin towards the shelves which ‘by-pass’ the buffering zone of the near-BSR zone where previously formed gas hydrate deposits act like a physical buffer limiting methane supply towards the upper parts of the GHSZ.

The modeling approach using methane generation kinetics based on Middelburg (1989) produces the best matches with the observed gas hydrate concentrations in the western Black Sea basin. Alternatively, we can recommend the use of temperature-dependent kinetics (Gaussian-type distribution) based on preliminary studies evaluating adequate temperature settings suitable for a region of interest. In the case of the western Black Sea basin, the best fit was obtained assuming a temperature window corresponding to the highest microbial activity at 30 °C–40 °C which remains consistent with the global studies on the biotic activity in marine sediments (Bradley et al., 2020; LaRowe et al., 2017, 2020).

Data statement

All data needed to evaluate the conclusions in the paper are presented in the paper and in the Appendix. The modeling results on the present-day and past basin-wide gas hydrate distributions are available as ASCII files stored in the online Supplementary Material.

CRediT authorship contribution statement

Ewa Burwicz-Galerie: Writing – review & editing, Writing – original draft, Visualization, Validation, Software, Resources, Methodology, Investigation, Formal analysis, Data curation, Conceptualization. **Matthias Haeckel:** Writing – review & editing, Validation, Software, Investigation, Funding acquisition, Formal analysis, Data curation. **Christian Hensen:** Writing – review & editing, Software, Investigation, Funding acquisition. **Rohit Samant:** Writing – review & editing, Investigation. **Klaus Wallmann:** Writing – review & editing, Investigation, Funding acquisition.

Declaration of competing interest

The authors declare that they have no known competing financial interests or personal relationships that could have appeared to influence the work reported in this paper.

Data availability

All data needed to evaluate the results are presented in the paper and in the Appendix. Present-day and past gas hydrate distributions are available as ASCII files in the Supplementary Material.

Appendix A

In this appendix, we explore various scenarios of organic matter generation depending on the kinetic rates used in the model. The reference scenario presented in the main part of this study is based on the Middelburg kinetics (Middelburg, 1989) widely used in the previous gas hydrate modeling studies (Burwicz et al., 2011, 2017; Burwicz and Rupke, 2019; Gupta et al., 2023; Schmidt et al., 2022; Wallmann et al., 2012). The alternative scenarios assume temperature-dependent Gaussian-type distribution of organic matter (OM) reactivity. Temperature values reported in Tables A.1 and A.2 refer to the peak temperature of each formulation.

Sensitivity of methane predictions to biogenic CH_4 generation kinetics

Based on the Gaussian temperature distribution kinetics, multiple numerical simulations were performed to examine the variability in the amount of biogenic and total methane generated in the western Black Sea basin. Using various temperature limits of microbial methanogenesis with the main activity peaks ranging from 30 °C to 70 °C, we investigated the influence of modeled methanogenesis on biogenic and total methane generation, migration and expulsion in the system. On the basis of the Middelburg kinetics, cumulative biogenic and total methane gas (biogenic and thermogenic) generated in the basin are estimated to be ~4,486 and ~6,427 GtC (see Tab. A1-2).

Based on our runs, generation of biogenic and total methane generally increases with a decrease in the peak temperature limit of the Gaussian distribution kinetics (see Fig. A.1). Cumulative biogenic and total methane generation from the low-temperature runs of 30 °C and 40 °C are the most consistent with the biogenic methane gas generated with the Middelburg run. This suggests that biogenic generation kinetics above 40 °C (based on the Gaussian-type of activity with a standard deviation set to a default number of 10 °C), usually underestimate methane generation on a basin-scale in the Black Sea system.

Table A.1

Cumulative biogenic methane generation balance for all sensitivity tests thorough the basin history

OM degradation model (peak temperature)	Generation Balance* (Gt CH_4)	Generated by primary cracking (Gt CH_4)	Generated by secondary cracking (Gt CH_4)	Cracked by secondary cracking (Gt CH_4)
Middelburg	4,486.14	4,542.21	13,938.84	-13,994.92
30 °C	4,400.96	4,443.25	12,535.73	-12,578.02
40 °C	4,318.84	4,356.90	11,905.17	-11,943.22
50 °C	4,233.65	4,268.87	11,378.83	-11,414.05
60 °C	4,148.36	4,180.08	10,876.16	-10,907.88
70 °C	4,054.91	4,084.24	10,245.09	-10,274.43

* Generation balance stands for the amount of biogenic methane cracked by primary cracking + generated by secondary cracking – cracked by secondary cracking.

Table A.2

Cumulative total methane generation (biogenic and thermogenic) for all sensitivity tests thorough the basin history

OM degradation model (peak temperature)	Generation Balance* (Gt CH_4)	Generated by primary cracking (Gt CH_4)	Generated by secondary cracking (Gt CH_4)	Cracked by secondary cracking (Gt CH_4)
Middelburg	6,427.42	5,004.81	15,417.52	-13,994.92
30 °C	6,329.95	4,902.78	14,005.19	-12,578.02
40 °C	6,234.82	4,813.29	13,364.75	-11,943.22
50 °C	6,139.16	4,722.73	12,830.48	-11,414.05
60 °C	6,045.16	4,631.80	12,321.23	-10,907.88
70 °C	5,941.67	4,533.44	11,682.65	-10,274.43

* Generation balance stands for the total amount of methane cracked by primary cracking + generated by secondary cracking – cracked by secondary cracking.

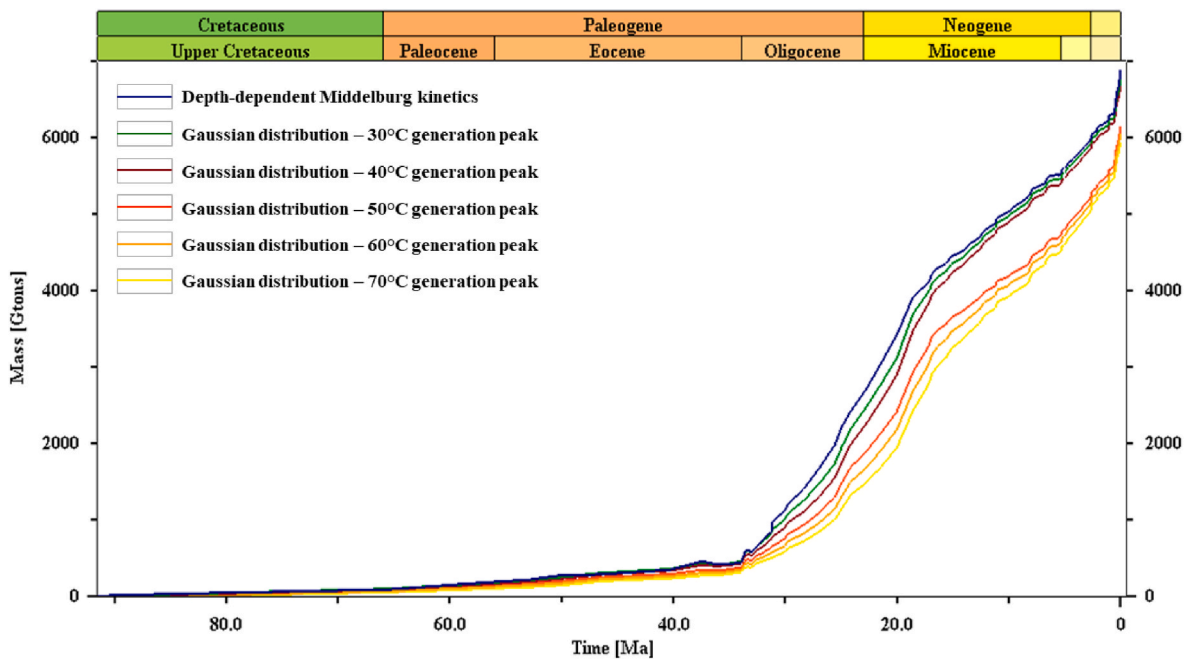


Fig. A.1. Cumulative generation of petroleum system components (oil, thermogenic, and biogenic methane) in the western Black Sea simulated using various biogenic methane generation kinetics.

For all the simulations, biogenic and thermogenic methane generation increases slowly and steadily until approximately 33 Ma with the peak productivity taking place from 33 Ma to 19 Ma which coincides with the presence of organic-rich Maykop formation (see Fig. A.1). Interestingly, two distinct generation trends of low-temperature (30 °C, 40 °C, and Middelburg) vs. high-temperature (50 °C, 60 °C, and 70 °C) results can be observed. Temperature control on biogenic methane generation starts to play a significant role about 33 Ma ago, however only about 19 Ma ago, the above mentioned two separate trends start to visibly split (see Fig. A.1). Overall, the rates of methane generation remain rather unified through time for all sensitivity scenarios, besides a time window starting at Late Eocene until Early Miocene, which reflects the dominant contribution of the Maykopian formation to the total hydrocarbon budget.

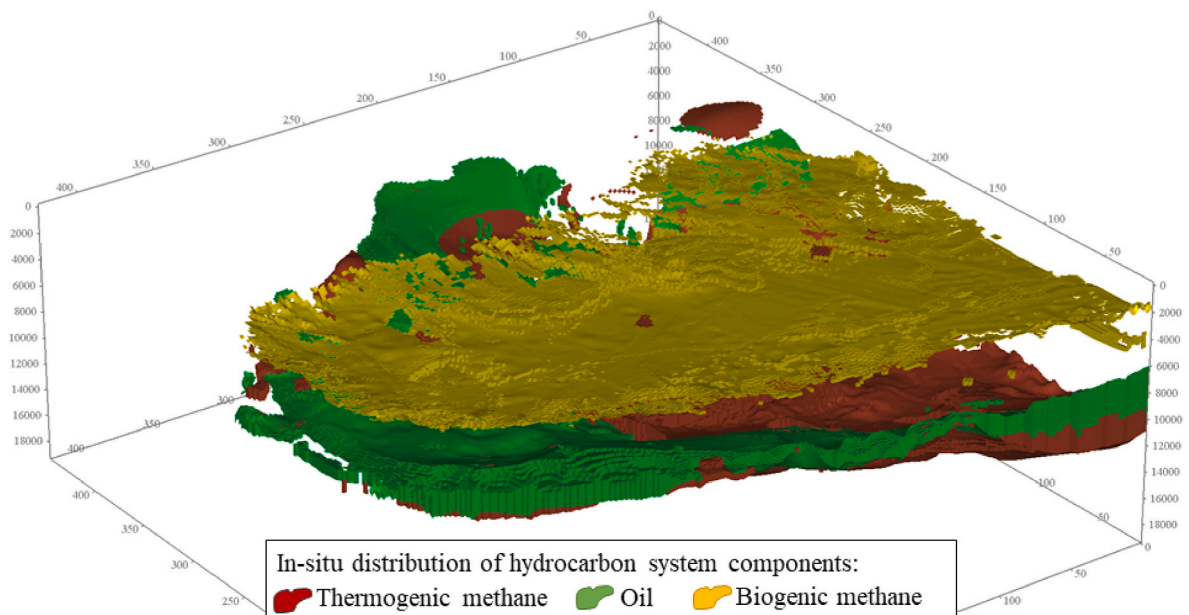


Fig. A.2. Basin-scale distribution of in-situ petroleum system components at the present-day, i.e. thermogenic methane (red), oil (green), and biogenic methane (yellow), generated for the Middelburg degradation kinetics.

The distribution of the petroleum system components (oil, thermogenic, and biogenic methane) is presented in Fig. A.2. Although the major generation of thermogenic components is predicted in the central (therefore more mature) part of the basin, long-distance migration towards the shelf areas plays a significant role in re-distributing these components.

Appendix A. Supplementary data

Supplementary data to this article can be found online at <https://doi.org/10.1016/j.marpetgeo.2024.107026>.

References

- Aydin, H., Merey, S., 2021. The effect of gas production from deeper conventional gas reservoirs on shallower gas hydrate layer stability: a case study in the conditions of the Sakarya gas field, Western Black Sea. *J. Nat. Gas Sci. Eng.* 94 <https://doi.org/10.1016/j.jngse.2021.104103>.
- Bahr, A., Arz, H.W., Lamy, F., Wefer, G., 2006. Late glacial to Holocene paleoenvironmental evolution of the Black Sea, reconstructed with stable oxygen isotope records obtained on ostracod shells. *Earth Planet. Sci. Lett.* 241 (3–4), 863–875. <https://doi.org/10.1016/j.epsl.2005.10.036>.
- Bialas, J., Bohlen, T., Dannowski, A., Eisenberg-Klein, G., Gassner, L., Gehrman, R., Heesch, K., Hölz, S., Jegen, M., Klaucke, I., Krieger, M., Mann, J., Müller, C., Prüssmann, J., Schicks, J., Schünemann, E., Schwalenberg, K., Sommer, M., Smilde, P.L., et al., 2020. Joint interpretation of geophysical field experiments in the Danube deep-sea fan, Black Sea. *Mar. Petrol. Geol.* 121 <https://doi.org/10.1016/j.marpetgeo.2020.104551>.
- Bialas, J., Haeckel, M., 2022. Gas hydrate accumulations in the Black Sea. In: Mienert, J. (Ed.), *World Atlas of Submarine Gas Hydrates in Continental Margins*. Springer, Nature Switzerland AG.
- Biaostoch, A., Treude, T., Rupke, L.H., Riebesell, U., Roth, C., Burwicz, E.B., Park, W., Latif, M., Boning, C.W., Madec, G., Wallmann, K., 2011. Rising Arctic Ocean temperatures cause gas hydrate destabilization and ocean acidification. *Geophys. Res. Lett.* 38, 5. <https://doi.org/10.1029/2011gl047222>.L08602.
- Boote, D.R.D., Sachsenhofer, R.F., Tari, G., Arbouille, D., 2018. Petroleum provinces of the PARATETHYAN region. *J. Pet. Geol.* 41 (3), 247–297. <https://doi.org/10.1111/jpg.12703>.
- Bradley, J.A., Arndt, S., Amend, J.P., Burwicz, E., Dale, A.W., Egger, M., LaRowe, D.E., 2020. Widespread energy limitation to life in global subseafloor sediments. *Sci. Adv.* 6 (32), 9. <https://doi.org/10.1126/sciadv.aba0697>.
- Burwicz, E., Haeckel, M., 2020. Basin-scale estimates on petroleum components generation in the Western Black Sea basin based on 3-D numerical modelling. *Mar. Petrol. Geol.* 113, 9. <https://doi.org/10.1016/j.marpetgeo.2019.104122>. Unsp104122.
- Burwicz, E., Reichel, T., Wallmann, K., Rottke, W., Haeckel, M., Hensen, C., 2017. 3-D basin-scale reconstruction of natural gas hydrate system of the Green Canyon, Gulf of Mexico. *G-cubed* 18 (5), 1959–1985. <https://doi.org/10.1002/2017gc006876>.
- Burwicz, E., Rupke, L., 2019. Thermal state of the Blake ridge gas hydrate stability zone (GHSZ)-Insights on gas hydrate dynamics from a new multi-phase numerical model. *Energies* 12 (17), 24. <https://doi.org/10.3390/en12173403>.3403.
- Burwicz, E.B., Rupke, L.H., Wallmann, K., 2011. Estimation of the global amount of submarine gas hydrates formed via microbial methane formation based on numerical reaction-transport modeling and a novel parameterization of Holocene sedimentation. *Geochem. Cosmochim. Acta* 75 (16), 4562–4576. <https://doi.org/10.1016/j.gca.2011.05.029>.
- Chazallon, B., Rodriguez, C.T., Ruffine, L., Carpentier, Y., Donval, J.P., Ker, S., Riboulot, V., 2021. Characterizing the variability of natural gas hydrate composition from a selected site of the Western Black Sea, off Romania. *Mar. Petrol. Geol.* 124 <https://doi.org/10.1016/j.marpetgeo.2020.104785>.104785.
- Colin, F., Ker, S., Riboulot, V., Sultan, N., 2020. Irregular BSR: evidence of an ongoing reequilibrium of a gas hydrate system. *Geophys. Res. Lett.* 47 (20) <https://doi.org/10.1029/2020gl089906>.e2020gl089906.
- Constantinescu, A.M., Toucanne, S., Dennielou, B., Jorry, S.J., Mulder, T., Lericolais, G., 2015. Evolution of the Danube deep-sea fan since the last glacial maximum: new insights into Black Sea water-level fluctuations. *Mar. Geol.* 367, 50–68. <https://doi.org/10.1016/j.margeo.2015.05.007>.
- Crutchley, G.J., Kroeger, K.F., Pecher, I.A., Mountjoy, J.J., Gorman, A.R., 2017. Gas hydrate formation amid submarine canyon incision: investigations from New Zealand's hikurangi subduction margin. *G-cubed* 18 (12), 4299–4316. <https://doi.org/10.1002/2017gc007021>.
- Dimitrov, L.I., 2002. Mud volcanoes - the most important pathway for degassing deeply buried sediments. *Earth Sci. Rev.* 59 (1–4), 49–76. [https://doi.org/10.1016/s0012-8252\(02\)00069-7](https://doi.org/10.1016/s0012-8252(02)00069-7).Pis0012-8252(02)00069-7.
- Dondurur, D., Küçük, H.M., Çifçi, G., 2013. Quaternary mass wasting on the western Black Sea margin, offshore of Amasra. *Global Planet. Change* 103, 248–260. <https://doi.org/10.1016/j.gloplacha.2012.05.009>.
- Duan, S.M., Hölz, S., Dannowski, A., Schwalenberg, K., Jegen, M., 2021. Study on gas hydrate targets in the Danube Paleo-Delta with a dual polarization controlled-source electromagnetic system. *Mar. Petrol. Geol.* 134 <https://doi.org/10.1016/j.marpetgeo.2021.105330>.105330.
- Erickson, J., A. Von Herzen, R.P., 1978. In: Ross, D.A., Neprochnov, Y.P. (Eds.), *Downhole Temperature Measurements and Heat Flow Data in the Black Sea - DSDP Leg 42B. Initial Reports of the Deep Sea Drilling Project*, pp. 1085–1103.
- Frye, M., Shedd, W., Boswell, R., 2012. Gas hydrate resource potential in the Terrebonne Basin, northern Gulf of Mexico. *Mar. Petrol. Geol.* 34 (1), 150–168. <https://doi.org/10.1016/j.marpetgeo.2011.08.001>.
- Fujii, T., Aung, T.T., Wada, N., Komatsu, Y., Suzuki, K., Ukita, T., Wygrala, B., Fuchs, T., Rottke, W., Egawa, K., 2016. Modeling gas hydrate petroleum systems of the Pleistocene turbiditic sedimentary sequences of the Daini-Atsumi area, eastern Nankai Trough, Japan. *Interpretation-A Journal of Subsurface Characterization* 4 (1), SA95–SA111. <https://doi.org/10.1190/int-2015-0022.1>.
- Gassner, L., Gerach, T., Hertweck, T., Bohlen, T., 2019. Seismic characterization of submarine gas-hydrate deposits in the Western Black Sea by acoustic full-waveform inversion of ocean-bottom seismic data. *Geophysics* 84 (5), B311–B324. <https://doi.org/10.1190/geo2018-0622.1>.
- GEBCO, Compilation, Group, 2023. *GEBCO 2023 Grid*, 10.5285/f98b053b-0c3c-6c23-e053-6c86abc0af7b. .
- Greiner, J., McGinnis, D.F., Naudts, L., Linke, P., De Batist, M., 2010. Atmospheric methane flux from bubbling seeps: spatially extrapolated quantification from a Black Sea shelf area. *Journal of Geophysical Research-Oceans* 115. <https://doi.org/10.1029/2009jc005381>.C01002.
- Grevemeyer, I., Villinger, H., 2001. Gas hydrate stability and the assessment of heat flow through continental margins. *Geophys. J. Int.* 145 (3), 647–660. <https://doi.org/10.1046/j.0956-540x.2001.01404.x>.
- Gupta, S., Burwicz-Galerner, E., Schmidt, C., Rüpke, L., 2023. Periodic states and their implications in gas hydrate systems. *Earth Planet. Sci. Lett.* 624 <https://doi.org/10.1016/j.epsl.2023.118445>.118445.
- Gupta, S., Deusner, C., Burwicz-Galerner, E., Haeckel, M., 2024. Numerical analysis of the dynamic gas hydrate system and multiple BSRs in the Danube paleo-delta, Black Sea. *Mar. Geol.* 469 <https://doi.org/10.1016/j.margeo.2024.107221>.
- Haeckel, M., Bialas, J., Klaucke, I., Wallmann, K., Bohrmann, G., Schwalenberg, K., Sugar participants, 2015. Gas hydrate occurrences in the Black Sea – new observations from the German SUGAR project. *Fire in the Ice: Methane Hydrate Newsletter* 2 (15), 6–9.
- Hantschel, T., Kauerauf, A.I., 2009. *Fundamentals of Basin and Petroleum Systems Modeling*. Springer-Verlag Berlin Heidelberg. <https://doi.org/10.1007/978-3-540-72318-9>.
- Hillman, J.I.T., Burwicz, E., Zander, T., Bialas, J., Klaucke, I., Feldman, H., Drexler, T., Awwiller, D., 2018a. Investigating a gas hydrate system in apparent disequilibrium in the Danube Fan, Black Sea. *Earth Planet. Sci. Lett.* 502, 1–11. <https://doi.org/10.1016/j.epsl.2018.08.051>.
- Hillman, J.I.T., Klaucke, I., Bialas, J., Feldman, H., Drexler, T., Awwiller, D., Atgin, O., Cifci, G., Badhani, S., 2018b. Gas migration pathways and slope failures in the Danube fan, Black Sea. *Mar. Petrol. Geol.* 92, 1069–1084. <https://doi.org/10.1016/j.marpetgeo.2018.03.025>.
- Hovland, M., 2002. On the self-sealing nature of marine seeps. *Continental Shelf Res.* 22 (16), 2387–2394. [https://doi.org/10.1016/s0278-4343\(02\)00063-8](https://doi.org/10.1016/s0278-4343(02)00063-8).Pis0278-4343(02)00063-8.
- Ivanov, M.K., Limonov, A.F., vanWeering, T.C.E., 1996. Comparative characteristics of the Black Sea and Mediterranean ridge mud volcanoes. *Mar. Geol.* 132 (1–4), 253–271. [https://doi.org/10.1016/0025-3227\(96\)00165-x](https://doi.org/10.1016/0025-3227(96)00165-x).
- Ker, S., Thomas, Y., Riboulot, V., Sultan, N., Bernard, C., Scalabrin, C., Ion, G., Marsset, B., 2019. Anomalously deep BSR related to a transient state of the gas hydrate system in the western Black Sea. *G-cubed* 20 (1), 442–459. <https://doi.org/10.1029/2018gc008761>.
- Kessler, J.D., Reeburgh, W.S., Southon, J., Seifert, R., Michaelis, W., Tyler, S.C., 2006. Basin-wide estimates of the input of methane from seeps and clathrates to the Black Sea. *Earth Planet. Sci. Lett.* 243 (3–4), 366–375. <https://doi.org/10.1016/j.epsl.2006.01.006>.
- Kretschmer, K., Biaostoch, A., Ruepke, L., Burwicz, E., 2015. Modeling the fate of methane hydrates under global warming. *Global Biogeochem. Cycles* 29 (5), 610–625. <https://doi.org/10.1002/2014gb005011>.
- Krezsek, C., Schleder, Z., Bega, Z., Ionescu, G., Tari, G., 2016. The Messinian sea-level fall in the western Black Sea: small or large? Insights from offshore Romania. *Petrol. Geosci.* 22 (4), 392–399. <https://doi.org/10.1144/petgeo2015-093>.
- Kroeger, K.F., Crutchley, G.J., Hill, M.G., Pecher, I.A., 2017. Potential for gas hydrate formation at the northwest New Zealand shelf margin - new insights from seismic reflection data and petroleum systems modelling. *Mar. Petrol. Geol.* 83, 215–230. <https://doi.org/10.1016/j.marpetgeo.2017.02.025>.
- Kroeger, K.F., Crutchley, G.J., Kellett, R., Barnes, P.M., 2019. A 3-D model of gas generation, migration, and gas hydrate formation at a Young Convergent margin (Hikurangi margin, New Zealand). *G-cubed* 20 (11), 5126–5147. <https://doi.org/10.1029/2019gc008275>.
- Kroeger, K.F., Plaza-Faverola, A., Barnes, P.M., Pecher, I.A., 2015. Thermal evolution of the New Zealand Hikurangi subduction margin: impact on natural gas generation and methane hydrate formation - a model study. *Mar. Petrol. Geol.* 63, 97–114. <https://doi.org/10.1016/j.marpetgeo.2015.01.020>.
- Kruglyakova, R.P., Byakov, Y.A., Kruglyakova, M.V., Chalenko, L.A., Shevtsova, N.T., 2004. Natural oil and gas seeps on the Black Sea floor. *Geo Mar. Lett.* 24 (3), 150–162. <https://doi.org/10.1007/s00367-004-0171-4>.
- LaRowe, D.E., Arndt, S., Bradley, J.A., Burwicz, E., Dale, A.W., Amend, J.P., 2020. Organic carbon and microbial activity in marine sediments on a global scale throughout the Quaternary. *Geochem. Cosmochim. Acta* 286, 227–247. <https://doi.org/10.1016/j.gca.2020.07.017>.
- LaRowe, D.E., Burwicz, E., Arndt, S., Dale, A.W., Amend, J.P., 2017. Temperature and volume of global marine sediments. *Geology* 45 (3), 275–278. <https://doi.org/10.1130/g38601.1>.
- Li, J., Haeckel, M., Dale, A.W., Wallmann, K., 2023. Degradation and accumulation of organic matter in euxinic surface sediments. *Geochem. Cosmochim. Acta.* <https://doi.org/10.1016/j.gca.2023.12.030>.
- Liu, J.L., Haeckel, M., Rutqvist, J., Wang, S.H., Yan, W., 2019. The mechanism of methane gas migration through the gas hydrate stability zone: insights from numerical simulations. *J. Geophys. Res. Solid Earth* 124 (5), 4399–4427. <https://doi.org/10.1029/2019jb017417>.
- Lüdmann, T., Wong, H.K., Konerding, P., Zillmer, M., Petersen, J., Flüß, E., 2004. Heat flow and quantity of methane deduced from a gas hydrate field in the vicinity of the Dnieper Canyon, northwestern Black Sea. *Geo Mar. Lett.* 24 (3), 182–193. <https://doi.org/10.1007/s00367-004-0169-y>.
- Lyu, C.F., Wang, X.X., Lu, X.S., Zhou, Q.S., Zhang, Y., Sun, Z.T., Xiao, L.M., Liu, X., 2020. Evaluation of hydrocarbon generation using structural and thermal modeling in the Thrust Belt of Kuqa Foreland basin, NW China. *Geofluids* 2020. <https://doi.org/10.1155/2020/8894030>.8894030.

- Mayer, J., Rupprecht, B.J., Sachsenhofer, R.F., Tari, G., Bechtel, A., Coric, S., Siedl, W., Kosi, W., Floodpage, J., 2018a. Source potential and depositional environment of Oligocene and Miocene rocks offshore Bulgaria. *Petroleum Geology of the Black Sea* 464, 307–328. <https://doi.org/10.1144/sp464.2>.
- Mayer, J., Sachsenhofer, R.F., Ungureanu, C., Bechtel, A., Gratzner, R., Sweda, M., Tari, G., 2018b. Petroleum charge and migration in the Black Sea: insights from oil and source rock geochemistry. *J. Pet. Geol.* 41 (3), 337–350. <https://doi.org/10.1111/jpg.12706>.
- Middelburg, J.J., 1989. A simple rate model for organic-matter decomposition in marine sediments. *Geochem. Cosmochim. Acta* 53 (7), 1577–1581. [https://doi.org/10.1016/0016-7037\(89\)90239-1](https://doi.org/10.1016/0016-7037(89)90239-1).
- Milkov, A.V., 2004. Global estimates of hydrate-bound gas in marine sediments: how much is really out there? *Earth Sci. Rev.* 66 (3–4), 183–197. <https://doi.org/10.1016/j.earscirev.2003.11.002>.
- Minshull, T.A., Marín-Moreno, H., Betlem, P., Bialas, J., Bünz, S., Burwicz, E., Cameselle, A.L., Cifcig, G., Giustiniani, M., Hillman, J.I.T., Hölz, S., Hopper, J.R., Ion, G., León, R., Magalhaes, V., Makovsky, Y., Mata, M.P., Max, M.D., Nielsen, T., Okay, S., Ostrovsky, I., O'Neill, N., Pinheiro, L.M., Plaza-Faverola, A.A., Rey, D., Roy, S., Schwalenberg, K., Senger, K., Vadakkepuliymbatta, S., Vasilev, A., Vázquez, J.T., 2020. Hydrate occurrence in Europe: a review of available evidence. *Mar. Petrol. Geol.* 111, 735–764. <https://doi.org/10.1016/j.marpetgeo.2019.08.014>.
- Monteleone, V., Minshull, T.A., Marín-Moreno, H., 2024. Seismic characterisation of multiple BSRs in the eastern Black Sea basin. *Mar. Petrol. Geol.* 161 <https://doi.org/10.1016/j.marpetgeo.2023.106604.106604>.
- Nasif, A., Ozel, F.E., Dondurur, D., 2020. Seismic identification of gas hydrates: a case study from Sakarya Canyon, western Black Sea. *Turk. J. Earth Sci.* 29 (3), 434–454. <https://doi.org/10.3906/yer-1909-2>.
- Naudts, L., Greinert, J., Artemov, Y., Beaubien, S.E., Borowski, C., De Batist, M., 2008. Anomalous sea-floor backscatter patterns in methane venting areas, Dnepr paleo-delta, NW Black Sea. *Mar. Geol.* 251 (3–4), 253–267. <https://doi.org/10.1016/j.margeo.2008.03.002>.
- Naudts, L., Greinert, J., Artemov, Y., Staels, P., Poort, J., Van Rensbergen, P., De Batist, M., 2006. Geological and morphological setting of 2778 methane seeps in the Dnepr paleo-delta, northwestern Black Sea. *Mar. Geol.* 227 (3–4), 177–199. <https://doi.org/10.1016/j.margeo.2005.10.005>.
- Nikishin, A.M., Okay, A.I., Tuysuz, O., Demir, A., Amelin, N., Petrov, E., 2015. The Black Sea basins structure and history: new model based on new deep penetration regional seismic data. Part 1: basins structure and fill. *Mar. Petrol. Geol.* 59, 638–655. <https://doi.org/10.1016/j.marpetgeo.2014.08.017>.
- Olaru, R., Krezsek, C., Rainer, T.M., Ungureanu, C., Turi, V., Ionescu, G., Tari, G., 2018. 3D basin modelling of oligocene - miocene maikop source rocks offshore Romania and in the western Black Sea. *J. Pet. Geol.* 41 (3), 351–365. <https://doi.org/10.1111/jpg.12707>.
- Özel, Ö., Dondurur, D., Klaucke, I., 2022. Seismic and geoaoustic evidence for subsurface fluid flow and seepage offshore Akcakoca, Southwestern Black Sea, Turkey. *Geo Mar. Lett.* 42 (4) <https://doi.org/10.1007/s00367-022-00740-z.17>.
- Pape, T., Blumenberg, M., Seifert, R., Bohrmann, G., Michaelis, W., 2008. Marine methane biogeochemistry of the Black Sea: a review. *Links between Geological Processes, Microbial Activities & Evolution of Life: Microbes and Geology* 4, 281.
- Pape, T., Haeckel, M., Riedel, M., Kolling, M., Schmidt, M., Wallmann, K., Bohrmann, G., 2020. Formation pathways of light hydrocarbons in deep sediments of the Danube deep-sea fan, Western Black Sea. *Mar. Petrol. Geol.* 122 <https://doi.org/10.1016/j.marpetgeo.2020.104627.104627>.
- Phrampus, B.J., Hornbach, M.J., Ruppel, C.D., Hart, P.E., 2014. Widespread gas hydrate instability on the upper U.S. Beaufort margin. *J. Geophys. Res. Solid Earth* 119 (12), 8594–8609. <https://doi.org/10.1002/2014jb011290>.
- Pinero, E., Hensen, C., Haeckel, M., Rottke, W., Fuchs, T., Wallmann, K., 2016. 3-D numerical modelling of methane hydrate accumulations using PetroMod. *Mar. Petrol. Geol.* 71, 288–295. <https://doi.org/10.1016/j.marpetgeo.2015.12.019>.
- Plaza-Faverola, A., Vadakkepuliymbatta, S., Hong, W.L., Mienert, J., Bünz, S., Chand, S., Greinert, J., 2017. Bottom-simulating reflector dynamics at Arctic thermogenic gas provinces: an example from Vestnesa Ridge, offshore west Svalbard. *J. Geophys. Res. Solid Earth* 122 (6), 4089–4105. <https://doi.org/10.1002/2016jb013761>.
- Popescu, I., De Batist, M., Lericolais, G., Nouze, H., Poort, J., Panin, N., Versteeg, W., Gillet, H., 2006. Multiple bottom-simulating reflections in the Black Sea: potential proxies of past climate conditions. *Mar. Geol.* 227 (3–4), 163–176. <https://doi.org/10.1016/j.margeo.2005.12.006>.
- Popescu, I., Lericolais, G., Panin, N., De Batist, M., Gillet, H., 2007. Seismic expression of gas and gas hydrates across the western Black Sea. *Geo Mar. Lett.* 27 (2–4), 173–183. <https://doi.org/10.1007/s00367-007-0068-0>.
- Reeburgh, W.S., Ward, B.B., Whalen, S.C., Sandbeck, K.A., Kilpatrick, K.A., Kerkhof, L.J., 1991. BLACK-SEA methane geochemistry. *Deep-Sea Res., Part A* 38, S1189–S1210.
- Riboulot, V., Cattaneo, A., Scalabrin, C., Gaillot, A., Jouet, G., Ballas, G., Marsset, T., Garziglia, S., Ker, S., 2017. Control of the geomorphology and gas hydrate extent on widespread gas emissions offshore Romania. *Bull. Soc. Geol. Fr.* 188 (4), 12. <https://doi.org/10.1051/bsgf/2017182.Unsp26>.
- Riedel, M., Bialas, J., Villinger, H., Pape, T., Haeckel, M., Bohrmann, G., 2021a. Heat flow measurements at the danube deep-sea fan, western Black Sea. *Geosciences* 11 (6). <https://doi.org/10.3390/geosciences11060240.240>.
- Riedel, M., Freudenthal, T., Bialas, J., Papenberg, C., Haeckel, M., Bergenthal, M., Pape, T., Bohrmann, G., 2021b. In-situ borehole temperature measurements confirm dynamics of the gas hydrate stability zone at the upper Danube deep sea fan, Black Sea. *Earth Planet Sci. Lett.* 563 <https://doi.org/10.1016/j.epsl.2021.116869.116869>.
- Riedel, M., Hahnel, L., Bialas, J., Bachmann, A.K., Gaide, S., Wintersteller, P., Klaucke, I., Bohrmann, G., 2021c. Controls on gas emission distribution on the continental slope of the western Black Sea. *Front. Earth Sci.* 8 <https://doi.org/10.3389/feart.2020.601254.601254>.
- Robinson, A.G., Rudat, J.H., Banks, C.J., Wiles, R.L.F., 1996. Petroleum geology of the Black Sea. *Mar. Petrol. Geol.* 13 (2), 195–223. [https://doi.org/10.1016/0264-8172\(95\)00042-9](https://doi.org/10.1016/0264-8172(95)00042-9).
- Römer, M., Sahling, H., Ferreira, C.D., Bohrmann, G., 2020. Methane gas emissions of the Black Sea-mapping from the Crimean continental margin to the Kerch Peninsula slope. *Geo Mar. Lett.* 40 (4), 467–480. <https://doi.org/10.1007/s00367-019-00611-0>.
- Sachsenhofer, R.F., Popov, S.V., Bechtel, A., Coric, S., Francu, J., Gratzner, R., Grunert, P., Kotarba, M., Mayer, J., Pupp, M., Rupprecht, B.J., Vincent, S.J., 2018. Oligocene and Lower Miocene source rocks in the Paratethys: palaeogeographical and stratigraphic controls. *Petroleum Geology of the Black Sea* 464, 267–306. <https://doi.org/10.1144/sp464.1>.
- Schmale, O., Haeckel, M., McGinnis, D.F., 2011. Response of the Black Sea methane budget to massive short-term submarine inputs of methane. *Biogeosciences* 8 (4), 911–918. <https://doi.org/10.5194/bg-8-911-2011>.
- Schmidt, C., Gupta, S., Rupke, L., Burwicz-Galerne, E., Hartz, E.H., 2022. Sedimentation-driven cyclic rebuilding of gas hydrates. *Mar. Petrol. Geol.* 140 <https://doi.org/10.1016/j.marpetgeo.2022.105628.105628>.
- Schwalenberg, K., Gehrman, R.A.S., Bialas, J., Rippe, D., 2020. Analysis of marine controlled source electromagnetic data for the assessment of gas hydrates in the Danube deep-sea fan, Black Sea. *Mar. Petrol. Geol.* 122 <https://doi.org/10.1016/j.marpetgeo.2020.104650.104650>.
- Starostenko, V.I., Dolmaz, M.N., Kutas, R.I., Rusakov, O.M., Oksum, E., Hisarlı, Z.M., Okay, M., Kalyoncuoglu, U.Y., Tutunsarar, H.E., Legostaeva, O.V., 2014. Thermal structure of the crust in the Black Sea: comparative analysis of magnetic and heat flow data. *Marine Geophysical Research* 35 (4), 345–359. <https://doi.org/10.1007/s11001-014-9224-x>.
- Starostenko, V.I., Rusakov, O.M., Shnyukov, E.F., Kobolev, V.P., Kutas, R.I., 2010. Methane in the northern Black Sea: characterization of its geomorphological and geological environments. *Sedimentary Basin Tectonics from the Black Sea and Caucasus to the Arabian Platform* 340, 57–75. <https://doi.org/10.1144/sp340.5>.
- Tari, G., Fallah, M., Schell, C., Kosi, W., Bati, Z., Sipahioğlu, N.O., Krezsek, C., Schleder, Z., Kozhuharov, E., Kitchka, A., 2016. Why are there no Messinian evaporites in the Black Sea? *Petrol. Geosci.* 22 (4), 381–391. <https://doi.org/10.1144/petgeo2016-003>.
- Treude, T., Krause, S., Steinle, L., Burwicz, E., Hamdan, L.J., Niemann, H., Feseker, T., Liebtrau, V., Krastel, S., Berndt, C., 2020. Biogeochemical consequences of nonventilating methane transport in sediment offshore northwestern svalbard. *J. Geophys. Res.-Biogeosci.* 125 (3), 26. <https://doi.org/10.1029/2019jg005371>. e2019JG005371.
- Vassilev, A., Dimitrov, L., 2002. Spatial and quantitative evaluation of the Black Sea gas hydrates. *Geofiz.* 43 (7), 672–684.
- Wallmann, K., Pinero, E., Burwicz, E., Haeckel, M., Hensen, C., Dale, A., Ruepke, L., 2012. The global inventory of methane hydrate in marine sediments: a theoretical approach. *Energies* 5 (7), 2449–2498.
- Wallmann, K., Riedel, M., Hong, W.L., Patton, H., Hubbard, A., Pape, T., Hsu, C.W., Schmidt, C., Johnson, J.E., Torres, M.E., Andreassen, K., Berndt, C., Bohrmann, G., 2018. Gas hydrate dissociation off Svalbard induced by isostatic rebound rather than global warming. *Nat. Commun.* 9, 9. <https://doi.org/10.1038/s41467-017-02550-9.83>.
- Winguth, C., Wong, H.K., Panin, N., Dinu, C., Georgescu, P., Ungureanu, G., Krugiakov, V.V., Podshuveit, V., 2000. Upper Quaternary water level history and sedimentation in the northwestern Black Sea. *Mar. Geol.* 167 (1–2), 127–146. [https://doi.org/10.1016/s0025-3227\(00\)00024-4](https://doi.org/10.1016/s0025-3227(00)00024-4).
- Xing, J.H., Spiess, V., 2015. Shallow gas transport and reservoirs in the vicinity of deeply rooted mud volcanoes in the central Black Sea. *Mar. Geol.* 369, 67–78. <https://doi.org/10.1016/j.margeo.2015.08.005>.
- Zander, T., Haeckel, M., Berndt, C., Chi, W.C., Klaucke, I., Bialas, J., Klaeschen, D., Koch, S., Atgm, O., 2017. On the origin of multiple BSRs in the Danube deep-sea fan, Black Sea. *Earth Planet Sci. Lett.* 462, 15–25. <https://doi.org/10.1016/j.epsl.2017.01.006>.
- Zander, T., Haeckel, M., Klaucke, I., Bialas, J., Klaeschen, D., Papenberg, C., Pape, T., Berndt, C., Bohrmann, G., 2020. New insights into geology and geochemistry of the Kerch seep area in the Black Sea. *Mar. Petrol. Geol.* 113 <https://doi.org/10.1016/j.marpetgeo.2019.104162.104162>.